Jörgen Teichter

Design of a shock tube

SP Swedish National Testing and Research Institute

SP Measurement Technology
SP REPORT 2005:35

Jörgen Teichter

Design of a shock tube

Abstract

A method is presented that models a shock tube with respect to pressure step amplitudes, maximum dwell-time and also including thin boundary layer theory.
It is a part of a project developing a primary method for dynamic calibration of pressure transducers with use of a shock tube.

The shock tube modelled in this report satisfies:

a) Combination of gases, Helium and Argon.
b) A side mounted measurement station satisfying maximum dwell time between the shock front and contact surface, ideal flow. The proposed distance where to place a side-mounted measurement station is $x_m = 1.6\ m$ from the diaphragm, driven section.
c) The range of pressure steps experienced by side-mounted (Δp_{21}) and end- mounted (Δp_{51}) pressure transducers, are given by
   i) $0.22 \le \Delta p_{21} \le 11 \quad (MPa)$, side-mounted measurement station.
   ii) $0.70 \le \Delta p_{51} \le 35 \quad (MPa)$, end-mounted measurement station.
d) Minimum total length and diameter of the shock tube producing thin turbulent boundary layer.
   The proposed minimum total length is $L = 5.0\ m$.
   The proposed length of the drive section is $l_T = 2.7\ m$.
   The proposed length of the driven section is $l_L = 2.3\ m$.
   The proposed minimum diameter is $D = 0.073\ m$.

Key words: shock tube, pressure, transducer, dynamic, calibration

SP Sveriges Provnings- och Forskningsinstitut
SP Rapport 2005:35
ISBN 91-85303-66-6
Borås 2005

SP Swedish National Testing and Research Institute
SP Report 2005:35

Postal address:
Box 857,
SE-501 15 BORÅS, Sweden
Telephone: +46 33 16 50 00
Telefax: +46 33 13 55 02
E-mail: info@sp.se
URL: http://www.sp.se

Contents

Denna sida (6) skall vara blank!

1 Introduction

A project devoted to different aspects of dynamic measurements is currently run by SP (Swedish National Testing and Research Institute), which includes the establishment of a network based in Sweden. One of the goals is to analyse the demands from Swedish industries[1] . The literature report by Hjelmgren[2] was the first study of existing methods and reported experiments related to dynamic measurements of pressure, for different ranges of amplitude, spectra and temperature. The need for calibration and uncertainty calculations were here discussed. As a part of a general ambition to develop traceable standards for dynamic measurement systems, this report focus on the design of shock tubes to be used for primary calibration of pressure transducers.

Pressure transducers are used for dynamic measurements where the reliability of obtained results is important. Measurements performed using two pressure transducers from different manufacturers should give similar results. For secondary comparison measurements, a method for primary dynamic characterization of reference transducers is needed. It is then necessary to have a device where not only a dynamic pressure can be realized but also accurately determined. It is also preferable to use pressure generators that resemble the actual measurement situation. Transducers used for measurements of impulsive pressures pulses may be characterized using a pressure step created by an aperiodic pressure generator. Among others, the shock tube is a realization of such a pressure generator[3]. This work is hence the first step to develop a primary method for dynamic calibration of pressure transducers, with the use of a shock tube. Besides this application, shock tubes are often used for studies of gas mixing, shock and air blast effects of nuclear weapons, boundary layer effects, validation of computer codes (computational gas-dynamics) and shock interaction.

This study consists of a determination of the size of a shock tube and its measurement positions where the pressure transducer under study can be mounted. Different choices of gases and pressure steps, as well as the dwell-time and the boundary layer will be studied and evaluated. Applying a one-dimensional theory, the following are taken into account:

i) Pressure step amplitudes.
ii) Coefficient of pressure step efficiency, as defined in this report.
iii) The dwell-time for a measurement point along the tube side is maximized, assuming ideal flow.
iv) The thin boundary layer theory developed by Mirels [9].

[1] [4].
[2] [4], pp. 29-32.
[3] [6], pp.49-58.

1.1 The shock tube

The uses of shock tubes in the studies of high temperature properties of gases were mostly developed during the 1950's and 1960's. A short summary of application areas until 1969 is given in [18]. Also in the development of chemical lasers and high-power gas dynamic, shock tubes are used as a device. Symposiums are held containing shock tube works and applications since 1957.

A conventional cylindrical shock tube consists of two sections separated by a diaphragm, driver section and driven section respectively, Fig 1-1.

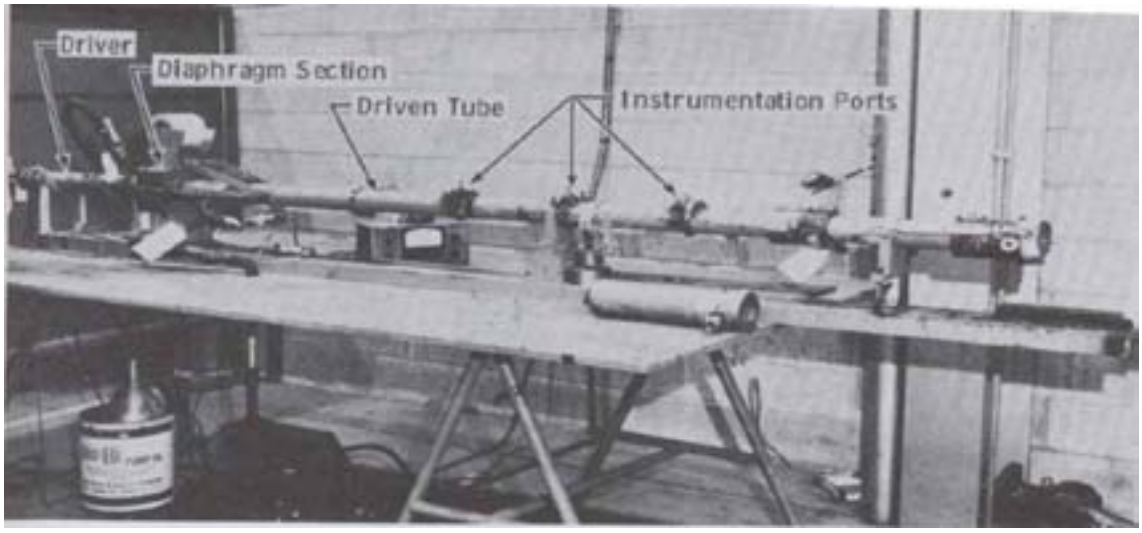

Figure 1-1 Photograph of shock tube **J** $_1$ ***[17].***

Each section contains gas initially held at different pressure. The type of gas could be the same or different in both sections. The drive section contains gas held at higher pressure than the driven section. Placing instrumentation on the long side or the end of the driven tube section can be made to perform e.g. measurements of pressures.

The course of events is as follows:

1. Gas/gases held at different pressures.
2. Rupture of the diaphragm.
3. Formation of a shock wave, an expansion wave and a contact surface.
4. Propagation of waves and the contact surface, Pt I.
5. Changes in gas conditions during the events of 4.
6. Due to the tube ends, reflection of waves.
7. Changes in gas condition during the events of 6.
8. Propagation of waves and the contact surface, Pt II.

2 Theory

This section explains the course of events inside a shock tube. It is a summary of a more detailed text presented in [1], [3] and [5] and pictures a one-dimensional simple shock tube.

2.1 Picture of a one-dimensional shock tube

2.1.1 Gas/gases held at different pressures

As an initial stage the two sections separated by a diaphragm will be filled with gas/gases held at different pressure, Fig. 2-1.

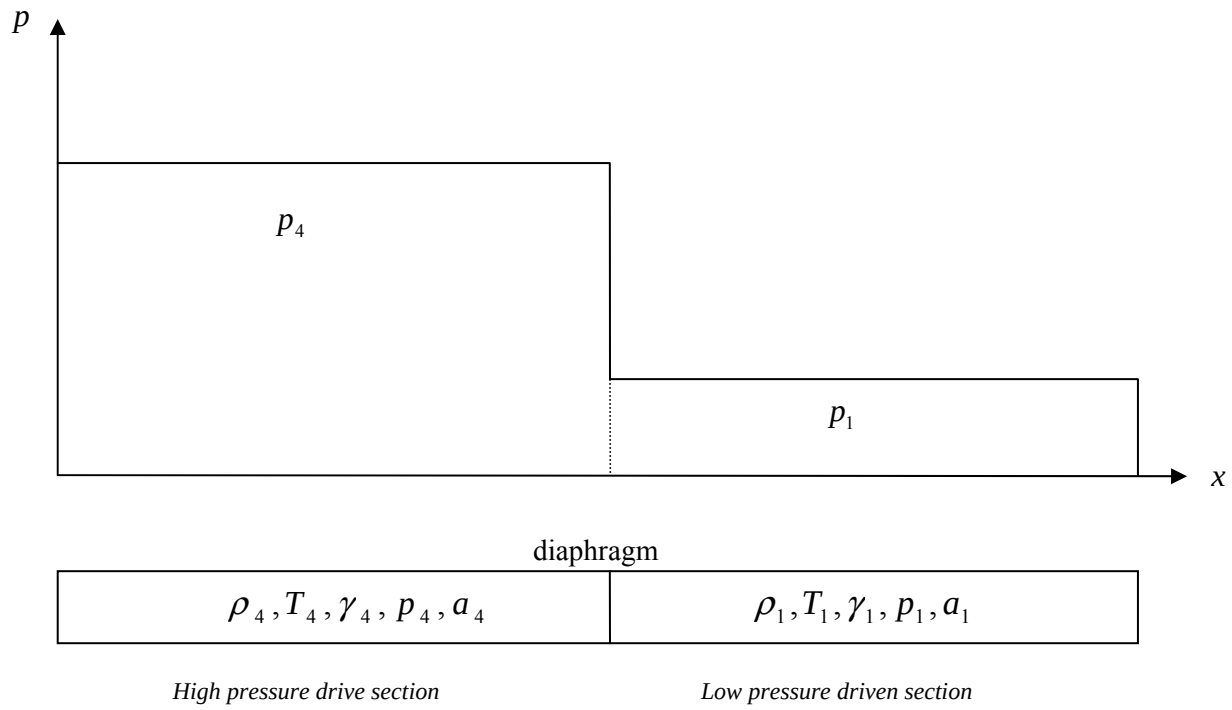

Figure 2-1 Pressure-driven shock tube held at initial condition.

The density, the temperature, the ratio of specific heat of capacity, the pressure and the speed of sound are denoted ρ, T, γ, p and a respectively. The combinations of gases that will be compared later on are:
He/N_2, He/Ar, N_2/Ar, He/Ne, Ne/N_2, Ne/Ar, He/He, N_2/N_2, Ar/Ar and Ne/Ne. These are gases "easy" to handle with respect to safety restriction.

2.1.2 Rupture of the diaphragm

The purpose is to create a shock wave by the breaking of the diaphragm. Different methods such as sharp cutting tools or the pressure itself can be used in combination with special designed diaphragm of different materials, [14]. Fig. 2-2 shows diaphragm made of stainless steel before and after the opening.

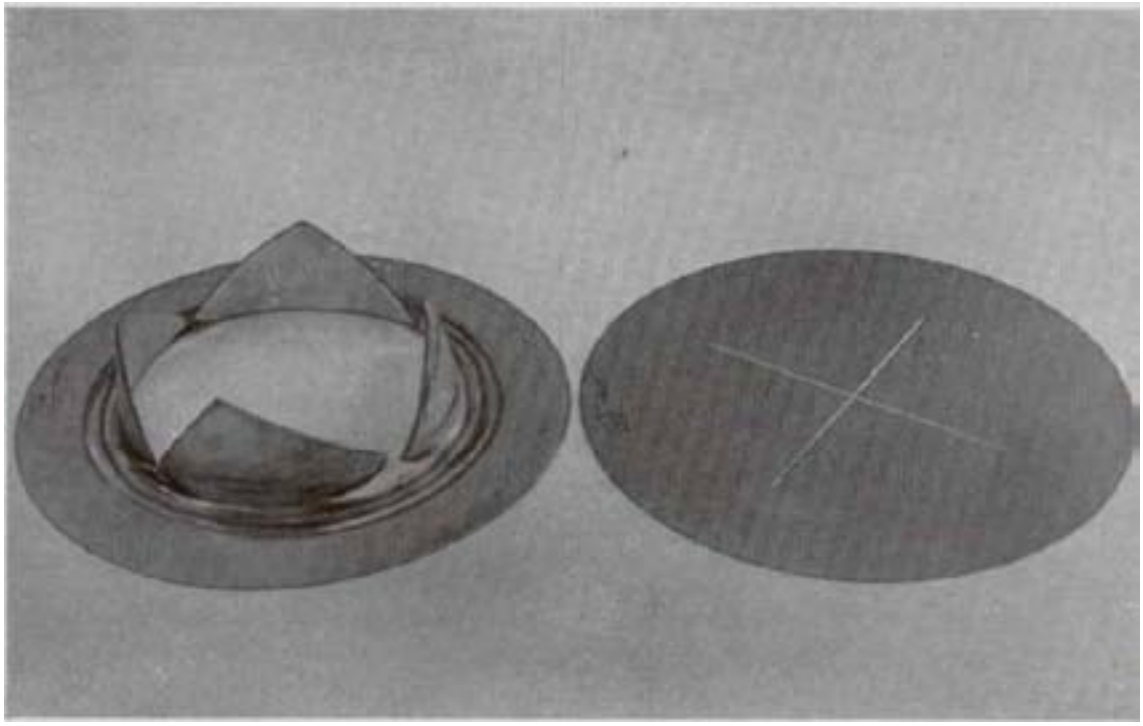

Figure 2-2 Diaphragm before and after opening [14].

Assume ideal diaphragm breaking for perfect gas conditions. Disturbances will affect neither the creation of waves or contact surface nor the flow.

2.1.3 Formation of shock wave, expansion wave and contact surface

Let $x = 0$ and $t = 0$ be placed where the diaphragm originally is placed, see Fig. 2-1.
Initially there is a pressure discontinuity ($p_4 > p_1$) at the origin and the physical solution will be compression waves and expansion waves moving in opposite direction[4].
A shock wave is created by a series of finite compression waves where the tail of the compression wave moves faster than the head. Finally they all coalesce into the incident shock wave.
In an expansion wave the head of the wave moves faster than the tail which means that an expansion wave disperses.
The creation of a contact surface is deduced from entropy consideration of the expansion and compression waves as a result of the increase of the entropy change during the growth of the shock front. Fig. 2-3 pictures the rupture of a diaphragm and the creation of waves and a contact surface.

---

[4] [5], p.48.

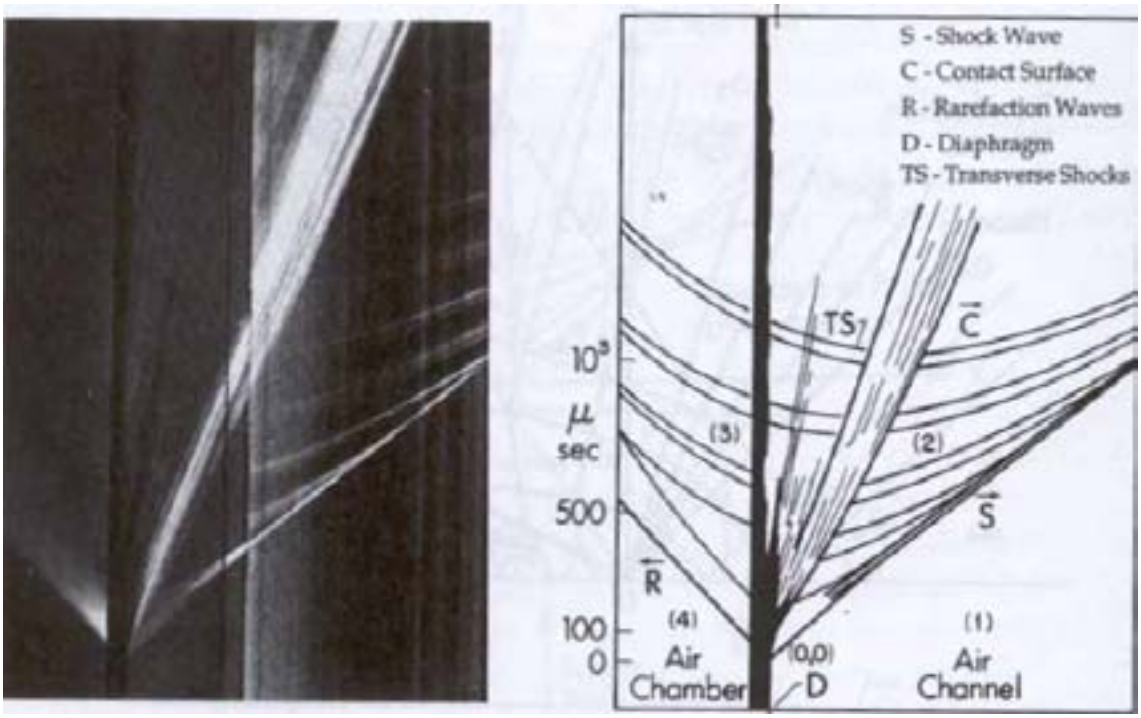

Figure 2-3 The wave system produced in a real shock tube from the instant the diaphragm ruptures [5].

If the condition of continuity across the contact surface with respect to the mass motion and pressure is to be satisfied, a centred reflected expansion wave has to be generated[5]. Boundary conditions across the contact surface are the pressures $p_3 = p_2$ and the velocities $u_3 = u_2 = u_p$, Fig. 2-4.

At the instant when the diaphragm is broken, assume immediate formation of a focused shock wave and that all wave elements start from the origin i.e. case of a centred expansion wave, a plane shock wave and a contact surface with constant thickness separating sections (2) and (3), i.e. no mixing of gases between sections (2) and (3) will occurs.

In Fig. 2-3 there are transverse waves created as well but from now on only the longitudinal waves will be considered.

[5] [5], p.35.

2.1.4 Propagation of waves and the contact surface, Pt I

After the diaphragm is ruptured, the shock wave S propagates into section (1) and an expansion wave E propagates into section (4). This is shown in Fig. 2-4.

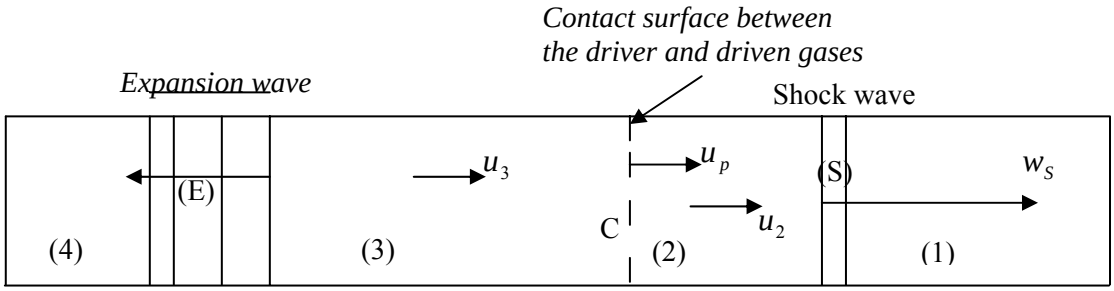

Figure 2-4 Propagation of waves and the contact surface after the rupture of the diaphragm, ideal case.

Let u and a denote the local values of mass velocity and speed of sound, respectively. The front of the expansion wave moves with a constant velocity a_4 to the left. The tail of the expansion wave moves with a constant velocity $u_3 - a_3$ to the right or left depending on whether $u_3 > a_3$ or not. The expansion wave will affect the drive gas conditions in (4) into a condition (3) and meantime induce a mass flow with the velocity u_3. In the driven section a shock wave is created and moves with a constant velocity $w_S > a_1$ and compresses the driven gas into a condition (2) and induces a mass motion with velocity u_2. The contact surface C moves with a constant velocity u_p.

2.1.5 Changes in gas conditions during the events of 2.1.4

The known quantities in the initial sections (4) and (1) will be used to find the unknown flow variables in the uniform states (2) and (3). For a calorically perfect gas the Riemann invariants[6] are constant through the expansion wave as well as the creation of the shock wave.
The process for the expansion wave is unsteady and isentropic and the equations of characteristics can be determined governing the differential equations of continuity and motion. The flow is isentropic and the pressure properties obtained by a centred expansion wave as a function of the local gas velocity, can be written[7] as

$$\frac{p_3}{p_4} = \left[1 - \frac{1}{f_4}\left(\frac{u_3}{a_4}\right)\right]^{2+f_4} \tag{1}$$

and $f = \dfrac{2}{\gamma - 1}$ is the number of degrees of freedom for a molecule with one or two atoms.
The shock wave process is equivalent to an irreversible, adiabatic, steady process and the equations of continuity, momentum, and energy are applied directly.

---

[6] Appendix A.
[7] Appendix A, Eq. A.45.

Assume the action of viscous and diabatic effects within the transition front only. The section (1) and (2) may then be considered to be in isentropic, one-dimensional states.[8]
Let the shock wave represent a discontinuity with zero-thickness and treat it as a jump between the section (1) and (2) with a change in entropy $\Delta s > 0$ across the shock wave.
Using the Rankine-Hugoniot equations for a normal shock wave the pressure ratio between section (1) and (2) has the relationship[9]

$$\frac{p_2}{p_1} = \frac{(1+f_1)\frac{\rho_2}{\rho_1} - 1}{(1+f_1) - \frac{\rho_2}{\rho_1}} \tag{2}$$

as a function of the density ratio.
Fig. 2-5 shows the development of pressure at an arbitrary time t after the breakage of diaphragm.

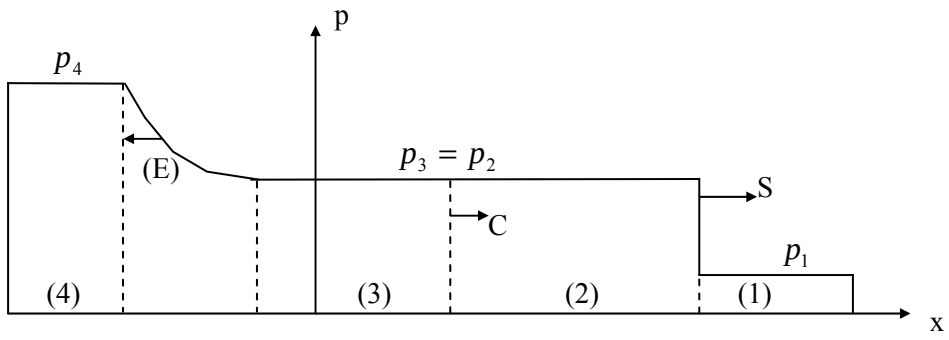

Figure 2-5 Development of pressure, ideal flow.

At the contact surface $p_3 = p_2, u_p = u_2 = u_3$ and the ratio p_2 / p_1 may be expressed as an implicit function of the diaphragm pressure ratio[10].

$$\frac{p_4}{p_1} = \frac{p_2}{p_1}\left[1 - \frac{\frac{f_1 a_1}{f_4 a_4}\left(\frac{p_2}{p_1} - 1\right)}{(2+f_1)\sqrt{1 + \frac{1+f_1}{2+f_1}\left(\frac{p_2}{p_1} - 1\right)}}\right]^{-(2+f_4)} \tag{3}$$

Relationship concerning; a centred expansion wave are stated in Table A-5, a compressing shock wave in Table A-1 and a moving normal shock wave in Table A-2.

---

[8] [5], p.37.
[9] Appendix A, Table A-1.
[10] Appendix A, using Eqs. A.20-21 and A.46.

2.1.6 Due to tube ends, reflection of waves

The propagating waves will strike the tube ends and both the shock wave and the expansion wave will undergo a normal reflection. The end walls are considered to be solid.
In case of a normal reflection of the shock wave the boundary condition demands a mass motion of zero behind the reflected shock wave SR. The reflected shock wave will be treated as a discontinuity with zero-thickness based on the arguing as in case of an incident shock wave.
In case of a normal reflected expansion wave ER the boundary condition demands a mass motion of zero behind the reflected expansion wave. According to [5] there is a theoretical possible steady state behind the reflected expansion wave. For a diatomic gas the speed of the tail of the wave has to be less or equal to $2a_4$ and for a monoatomic gas, less or equal to a_4.

2.1.7 Changes in gas condition during the events of 2.1.6

Using the Rankine-Hugoniot equations for a reflected shock wave the pressure relations yields[11]

$$\frac{p_5 - p_1}{p_2 - p_1} = \frac{\rho_2}{\rho_1}\left(1 + \frac{w_{SR}}{w_S}\right) \tag{4}$$

as a function of the density ratio and the shock wave velocity ratio.

Fig. 2-6 shows the development of pressure at an arbitrary time t after the waves have been reflected.

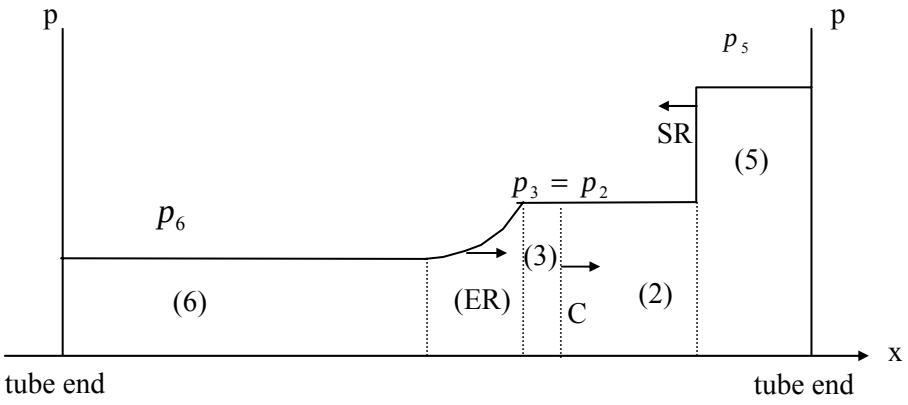

Figure 2-6 Development of pressure, ideal flow.

The pressure ratio between the pressure p_5 behind the reflected shock wave and the initial pressure p_1 may be expressed as[12]

$$\frac{p_5}{p_1} = \frac{(1 + k_{21})[(2 + f_1) + (3 + f_1)k_{21}]}{(2 + f_1) + k_{21}} \tag{5}$$

k_{21} is the shock strength and refers to the definition made in section (3.1.1).

The change of states in case of the reflected expansion wave is considered to be isentropic.

---

[11] Appendix A, Eq. A.26.
[12] Appendix A, using Table A-1 and A-3.

The pressure ratio between the pressure p_6 behind the reflected expansion wave and the initial pressure p_1 may be expressed as[13]

$$\frac{p_6}{p_1} = \frac{p_4}{p_1}\left[2\left(\frac{p_2}{p_4}\right)^{\frac{1}{2+f_4}} - 1\right]^{2+f_4} \tag{6}$$

and $\frac{p_2}{p_4} = \frac{p_2}{p_1} \cdot \frac{p_1}{p_4}$.

2.1.8 Propagation of waves and the contact surface, Pt II

To picture the development of waves in a shock tube one usually uses a Path (x)-Time (t) -diagram like the one in Fig. 2-7.

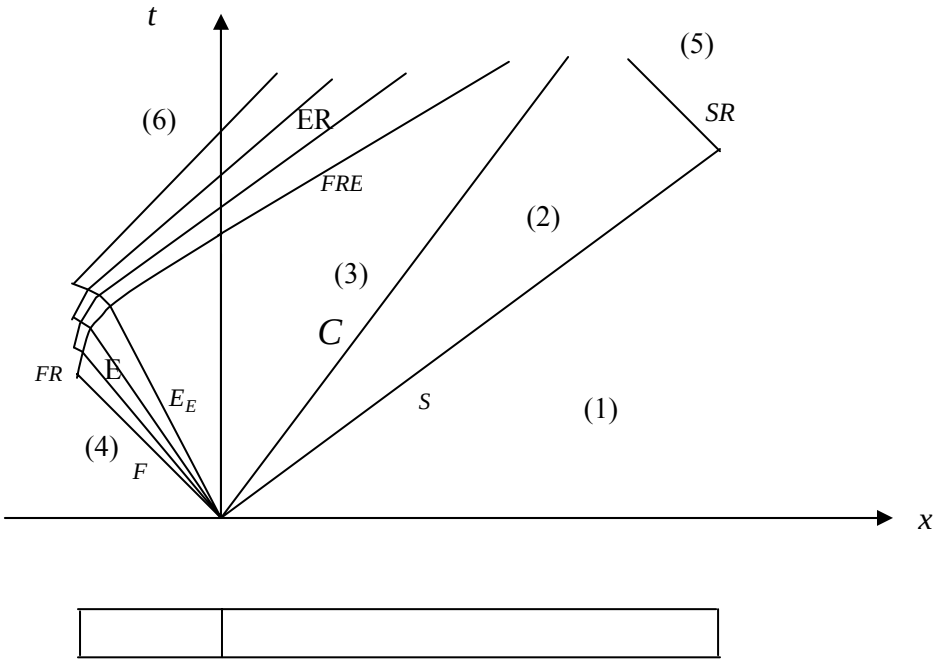

Figure 2-7 Path (x) – Time (t) –diagram showing the development of waves in a shock tube, ideal flow.

Origin represents $x = 0, t = 0$ where the diaphragm is situated when it's broken. After the rupture the shock wave S has the constant velocity w_S, the reflected shock wave SR has the constant velocity w_{SR}, the contact surface C has the constant velocity u_p, the tail of the expansion wave E_E has the constant velocity $u_{EE} = u_3 - a_3$ and the front of the expansion wave F has the constant velocity $u_F = -a_4$. ER is the reflected expansion wave and FR is the front of the reflected expansion wave moving with the constant velocity $u_{FR} = u_E + a_E > u_{EE}$. Finally, FRE is the result of FR coincides with E_E and will move with the constant velocity $u_{FRE} = u_3 + a_3$.

---

[13] Appendix A, Eq.A.51.

3 Method & Result

Contains optimization, design and handling of the shock tube.

3.1 Optimization

In section (3.1.1) pressure step is discussed and the shock strength is defined.
In section (3.1.2) the coefficient of pressure step efficiency is defined.
In section (3.1.3) the choice of gases is made with respect to the coefficient of pressure step efficiency and the shock strength is decided with respect to pressure step amplitude. The range of pressure steps is also discussed.
Finally, section (3.1.4) deals with relations satisfying maximum dwell-time along the tube side, ideal flow. The dwell-time at the tube end is briefly discussed.

3.1.1 The shock strength

With the assumption of a shock wave of zero-thickness there will be a pressure step between the sections (2) and (1), fig. 2-5. A transducer mounted at the sidewall will experience a pressure step $\Delta p_{21} = p_2 - p_1$. Moreover, a transducer mounted at the end wall will experience a pressure step $\Delta p_{51} = p_5 - p_1$, due to the reflection of the incident shock wave S transforming into SR, Fig. 2-6.
Relating Δp_{21} and Δp_{51} to the initial pressure p_1 and define the shock strength[14] k as

$$k_{ij} \equiv \Delta p_{ij} / p_j \tag{7}$$

gives

$$k_{21} = \frac{\Delta p_{21}}{p_1} \qquad k_{51} = \frac{\Delta p_{51}}{p_1} \tag{8}$$

The Mach number[15] for the incident shock wave is

$$M_S = \frac{w_S}{a_1} \tag{9}$$

and as a function of the shock strength[16] k_{21}

$$M_S{}^2 = \frac{(1+f_1)}{(2+f_1)} \cdot k_{21} + 1 \tag{10}$$

in case of a given f_1.

For different values of k_{21} there will be upper limits for possible pressure steps Δp_{21} and Δp_{51}. This means that the shock strength cannot be too small in order to achieve large pressure steps. This is shown in Fig. 3-1 below.

---

[14] [2], p.59.
[15] Appendix A, Eq. A.15.
[16] Appendix A, Eq. A.20.

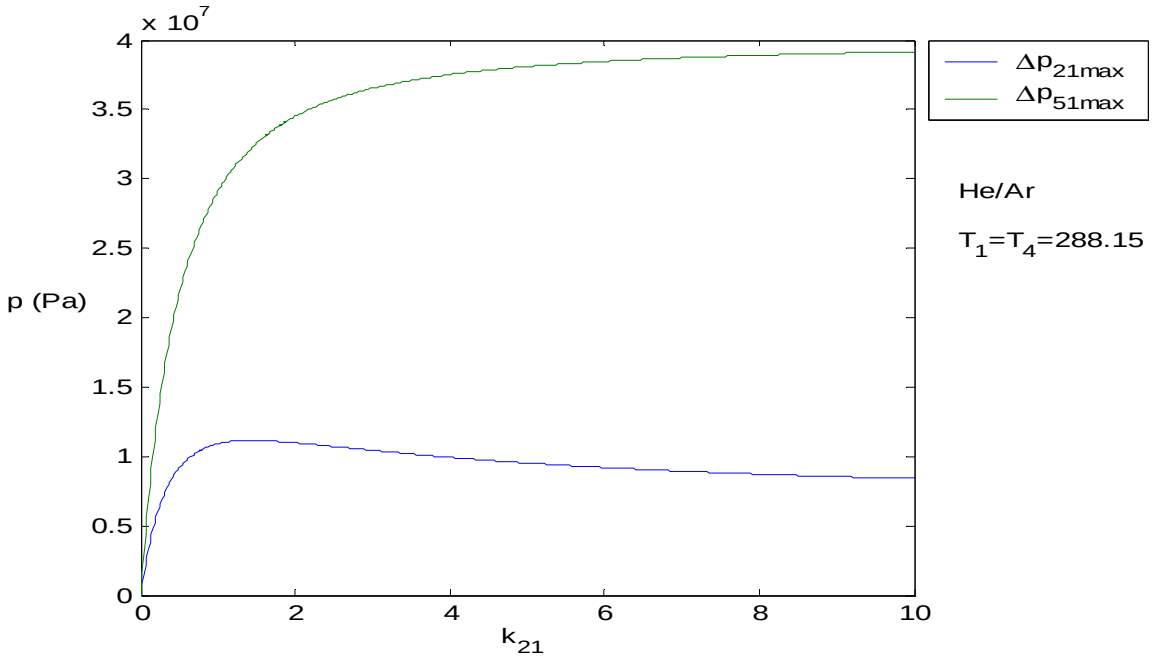

Figure 3-1 Pressure steps $\Delta p_{51\max}$ ***and*** $\Delta p_{21\max}$ ***plotted against the pressure strength*** k_{21}***. Helium drive gas, Argon driven gas. Let*** $p_{5\max} = 40MPa$***. With use of Eqs.C.1, C.3 and C.5*** $p_{1\max}(k_{21})$ ***is evaluated and values of*** $\Delta p_{51\max}(k_{21})$ ***and*** $\Delta p_{21\max}(k_{21})$ ***are obtained.***

In Appendix E graphs E1-E10, maximum pressure steps and maximum pressures are presented for different combinations of gases with respect to k_{21}.

Δp_{51} increases with higher value of k_{21} whereas there is a maximum value of Δp_{21}.

Using of Eqs. C.1,C.3,C.5 and the condition of $p_{5\max} = 40Mpa$, give the expression

$$\Delta p_{21} = \frac{p_{5\max}(\tilde{B} + k_{21})}{(1 + k_{21})(\tilde{B} + \tilde{C}k_{21})} \cdot k_{21} \tag{12}$$

and

$$\tilde{A} = 1 + f_1 \qquad \tilde{B} = 2 + f_1 \qquad \tilde{C} = 3 + f_1 \tag{12.a}$$

Maximum value of Δp_{21} is obtained by letting

$$\frac{d}{dk_{21}} \Delta p_{21} = 0 \tag{12.b}$$

solving for k_{21} yields

$$k_{21m} = \frac{\tilde{B}\left(1 + \sqrt{\tilde{A}\tilde{B}}\right)}{\tilde{B}\tilde{C} - (\tilde{B} + \tilde{C})} \tag{12.c}$$

positive root.

3.1.2 Coefficient of pressure step efficiency

The pressure steps are an outcome from the use of the shock tube. The shock tube is a device that generates pressure steps with a pressure ratio p_4 / p_1 as initial condition. It is a property that belongs to the shock tube, although the properties of chosen gas/gases will affect the initial condition.

Define the coefficient of pressure step efficiency as

$$c_{e,i} \equiv \frac{k_{ij}}{(p_4 / p_1)} \tag{13}$$

It relates the shock strength to the initial pressure ratio and the coefficient will be a measure of the efficiency, a property belonging to the shock tube as a device.

Graphs E11-E30 for different combinations of gases showing $c_{e,5}$ versus k_{51} and $c_{e,2}$ versus k_{21} are presented in Appendix E.

3.1.3 Choice of drive/driven gas and shock strength

The pressure steps of interest will be in a range between $100kPa$ and $100MPa$[17]. Restrictions due to safety lead to maximum pressure amplitude of $40Mpa$ in the driver and driven section respective.
That is $p_{4\max} \le p_{5\max} = 40Mpa$. Restriction of the length of the shock tube is up to 10 meters and the temperature at wall is assumed to be constant, $T = T_1 = T_4 = 288.15K$. The gas-combination will be chosen with respect to the coefficient of efficiency. The choice will be Helium as drive gas and Argon as driven gas, based on the condition $p_{5\max} = 40Mpa$ and mean values of $c_{e,5}$ and $c_{e,2}$ with respect to different values of k_{51} $(0 \le k_{51} \le k_{51}(k_{21} = 5))$ and k_{21} $(0 \le k_{21} \le 5)$, presented in Table 3-1 and Table 3-2 below. The value of $k_{21} = 5$ is set as an upper limit to ensure a theoretical steady state condition in section (6) for the combination of gases that are compared. Consideration in view of values of $c_{e,i}$ at $k_{21} = 2.18$ and $k_{51} = 7$ for He/Ar and He/N_2 was made as well.

[17] [4], p.23.

Table 3-1 Mean value of $c_{e,5}$ for different combinations of gases. Higher value is better efficiency with respect to the initial pressure ratio p_4 / p_1. Temperature $T = T_1 = T_4 = 288.15K$ and $p_{5\max} = 40MPa$.

He/Ar $k_{51} = 7$	Gas Drive/Driven	He/N_2	He/Ar	N_2/Ar	He/Ne	Ne/N_2
1.4	$c_{e,5}$	1.2	1.3	0.61	1.0	0.50

He/N_2 $k_{51} = 7$	Gas Drive/Driven	Ne/Ar	He/He	N_2/N_2	Ar/Ar	Ne/Ne
1.3	$c_{e,5}$	0.66	0.39	0.46	0.39	0.39

Table 3-2 Mean value of $c_{e,2}$ for different combinations of gases. Higher value is better efficiency with respect to the initial pressure ratio p_4 / p_1. Temperature $T = T_1 = T_4 = 288.15K$ and $p_{5\max} = 40MPa$.

He/Ar $k_{21} = 2.18$	Gas Drive/Driven	He/N_2	He/Ar	N_2/Ar	He/Ne	Ne/N_2
0.44	$c_{e,2}$	0.34	0.39	0.19	0.32	0.15

He/N_2 $k_{21} = 2.18$	Gas Drive/Driven	Ne/Ar	He/He	N_2/N_2	Ar/Ar	Ne/Ne
0.39	$c_{e,2}$	0.21	0.13	0.15	0.13	0.13

The idea is to keep k_{21} constant and vary the pressure p_1. Δp_{21} will act as a function of p_1 and Δp_{51} will act as a function of p_1 and f. For given f all quantities are expressed in a single variable, namely the initial pressure p_1. The relevant equations are listed in App. A, App C and App H.

If the pressure steps Δp_{51} were to be neglected, the choice of the shock strength k_{21} would be k_{21m}, Eq. 12.c. According to Fig. 3-1 there is a slow decrease of Δp_{21} for values of $k_{21} \geq k_{21m}$. On the contrary there is a slow increase of Δp_{51} for values of $\Delta p_{51} \geq 35MPa$.
The shock strength will be decided upon the pressure step $\Delta p_{51\max} = 35MPa$ with the constrain $p_{4\max} \leq p_{5\max} = 40Mpa$.
The shock strength $k_{21} = 2.18$ (Eq.14) satisfies $\Delta p_{51\max} = 35Mpa$, $p_{1\max} = 5MPa$ and $k_{51} = 7$ in Eq.8.

$$k_{21} = \frac{k_{51} - 2(2+f_1)}{2(3+f_1)} + \sqrt{\left(\frac{k_{51} - 2(2+f_1)}{2(3+f_1)}\right)^2 + \left(\frac{2+f_1}{3+f_1}\right)k_{51}} \qquad (14)$$

positive root.
Eq. 14 is obtained by use of Eq. C.3. Eq. 10 gives $M_S = 1.66$.

3.1.3.1 Range of pressure steps for $k_{21} = 2.18$ and $k_{51} = 7$

The initial pressure p_1 will be decided upon the proposed pressure step by use of Eq.8.
Let the constant pressure strength k_{21} act as a working coefficient. The characteristic functions presented in Fig. 3-2 shows the range of pressure steps obtained by the variation of the initial pressure p_1.

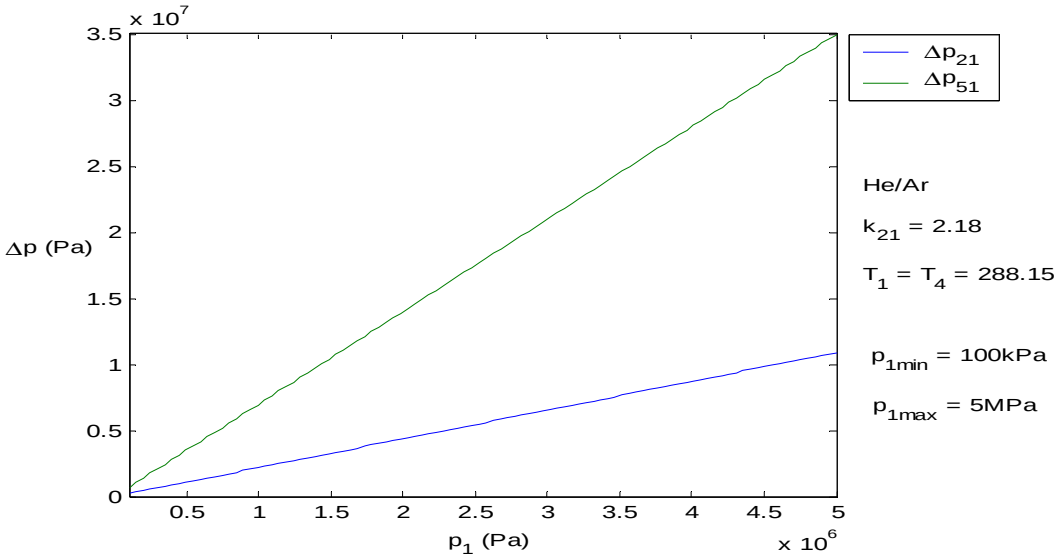

Figure 3-2 Range of pressure steps, Δp_{21} and Δp_{51}. $k_{21} = 2.18$, $k_{51} = 7$

Fig. 3-3 shows the characteristic functions of pressure range obtained by the variation of the initial pressure p_1.

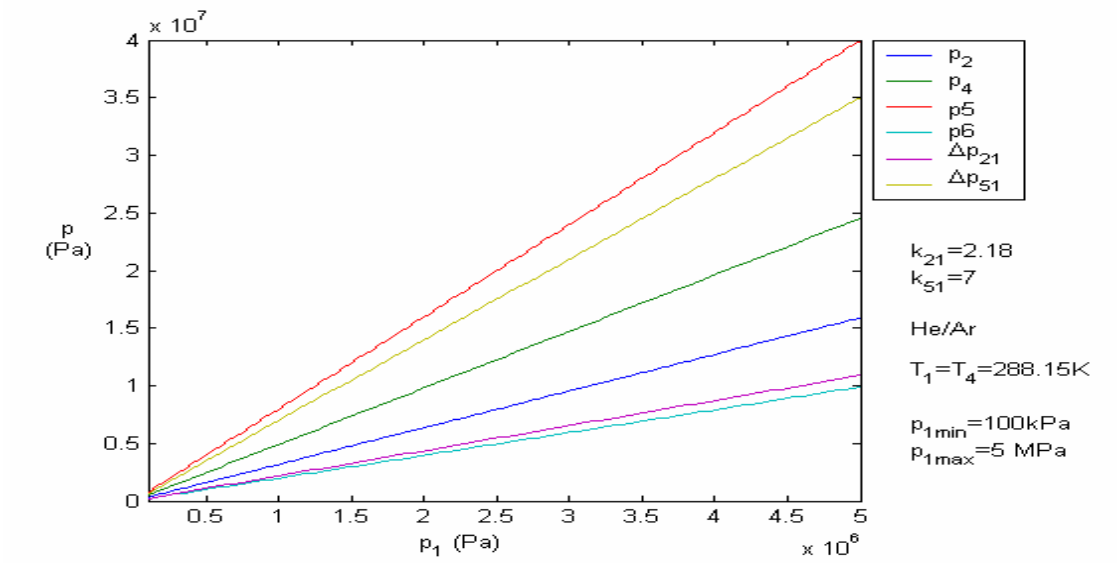

Figure 3-3 Pressure ranges obtained by the variation of the initial pressure p_1.

Minimum and maximum values of pressure are presented in Table 3-3 in accordance to Fig. 3-3.

Table 3-3 Minimum and maximum values of pressure.

Pressure (MPa)	$p_2 = p_3$	p_4	p_5	p_6	Δp_{21}	Δp_{51}
$p_{1\min} = 0.1$	0.32	0.49	0.80	0.20	0.22	0.70
$p_{1\max} = 5$	16	25	40	10	11	35

p_6 is the pressure in section (6) and p_5 is the pressure in section (5), Fig (2-6). The characteristic functions are

$$\begin{array}{lll} \frac{p_2}{p_1} = 3.2 & \frac{p_4}{p_1} = 4.9 & \frac{p_5}{p_1} = 8.0 \\ \frac{p_6}{p_1} = 2.0 & \frac{\Delta p_{21}}{p_1} = k_{21} = 2.2 & \frac{\Delta p_{51}}{p_1} = k_{51} = 7.0 \end{array} \qquad (15)$$

3.1.4 Maximum dwell-time for pressure measurements, ideal flow

The point where the maximum dwell-time at the sidewall occurs is determined. Also the dwell-time at the tube end is briefly discussed. For our purpose we want to maintain the pressure p_2 in section (2) behind the incident shock wave S and the pressure in section (5) behind the reflected shock wave SR, undisturbed as long as possible because these are the sections were the measuring are performed by our probes.

3.1.4.1 Sidewall

With use of Path (x)-Time (t) -diagrams it is possible to find the conditions of a maximum $\Delta_2 t$ maintaining section (2) undisturbed. This is done by argument text and with aid of Fig. 3-4 to Fig. 3-6. The time duration between the incident shock wave S passes the point x_{SRC} or x_{FREC} and the contact surface C reaching the same, is defined as the dwell-time $\Delta_2 t$.
Fig. 3-4 shows the case when the reflected shock wave SR reaches the contact surface C at time t_{SRC}, before the front of the reflected expansion wave FRE does.
Fig. 3-5 shows the case when the front of the reflected expansion wave FRE reaches the contact surface C at the time t_{FREC} and overtakes the contact surface before the reflected shock wave SR arrives. The front of the reflected expansion wave $FREC$ will continue with the constant velocity $u_{FREC} = u_2 + a_2 > w_S$ until it reaches the reflected shock wave SR.

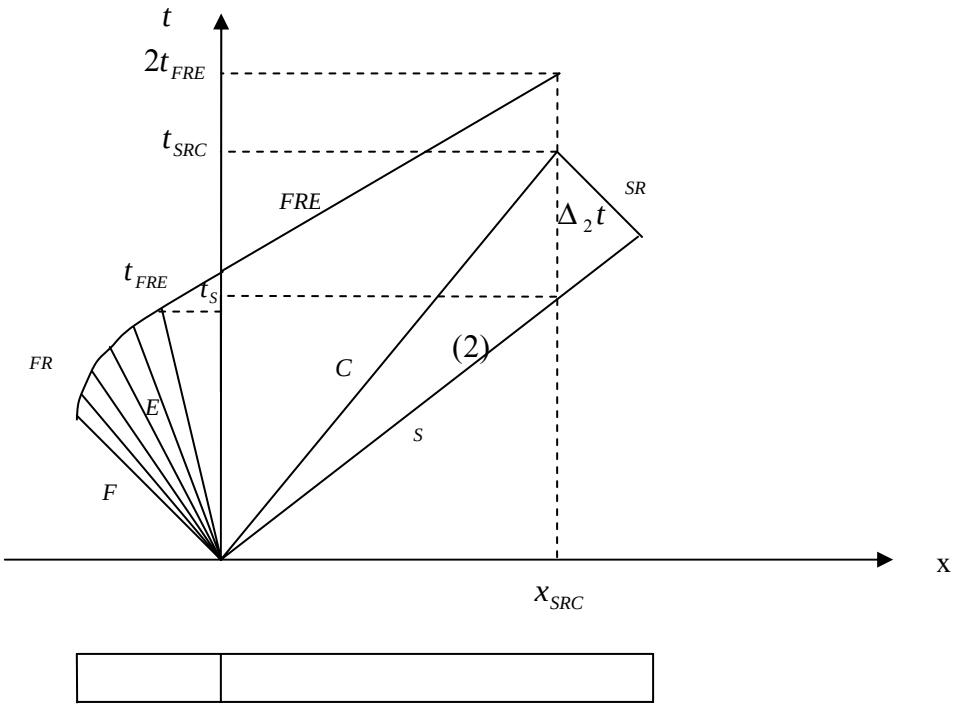

Figure 3-4 Path (x) ***-Time*** (t) ***-diagram in case where the reflected shock wave*** SR ***reaches the contact surface*** C ***at time*** t_{SRC} ***before the front of the reflected expansion wave*** FRE ***does.***

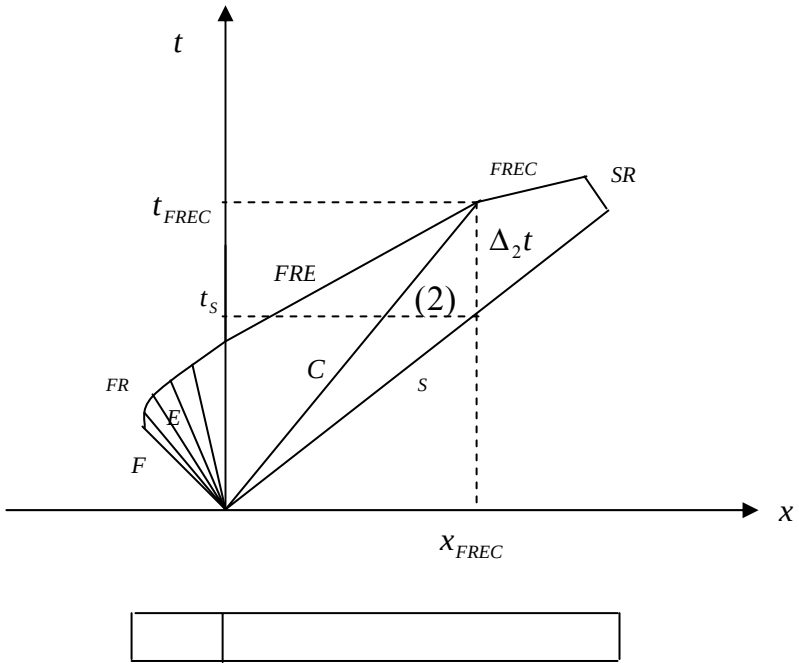

Figure 3-5 Path (x) ***-Time*** (t) ***-diagram in case where the front of the reflected expansion wave*** FRE ***reaches the contact surface*** C ***at time*** t_{FREC} ***before the reflected shock wave*** SR ***does.***

Take section (2) into consideration.

From Fig. 3-4, the largest time $\Delta_2 t = t_{SRC} - t_S$ is at the point x_{SRC}.

From Fig. 3-5, the largest time $\Delta_2 t = t_{FREC} - t_S$ is at the point x_{FREC}.
It can be deduced from the figures that maximum $\Delta_2 t$ occurs where the time t_{FREC} is increased up till the time t_{SRC} occurs and in meanwhile the time t_{SRC} is increased up till the time $2t_{FRE}$ occurs. Maximum $\Delta_2 t$ occurs at the point where x_{SRC} coincides with x_{FREC} and $t_{FREC} = t_{SRC} = 2t_{FRE}$.
The derivation of this relation is done in App. D.
This situation is pictured in Fig. 3-6.

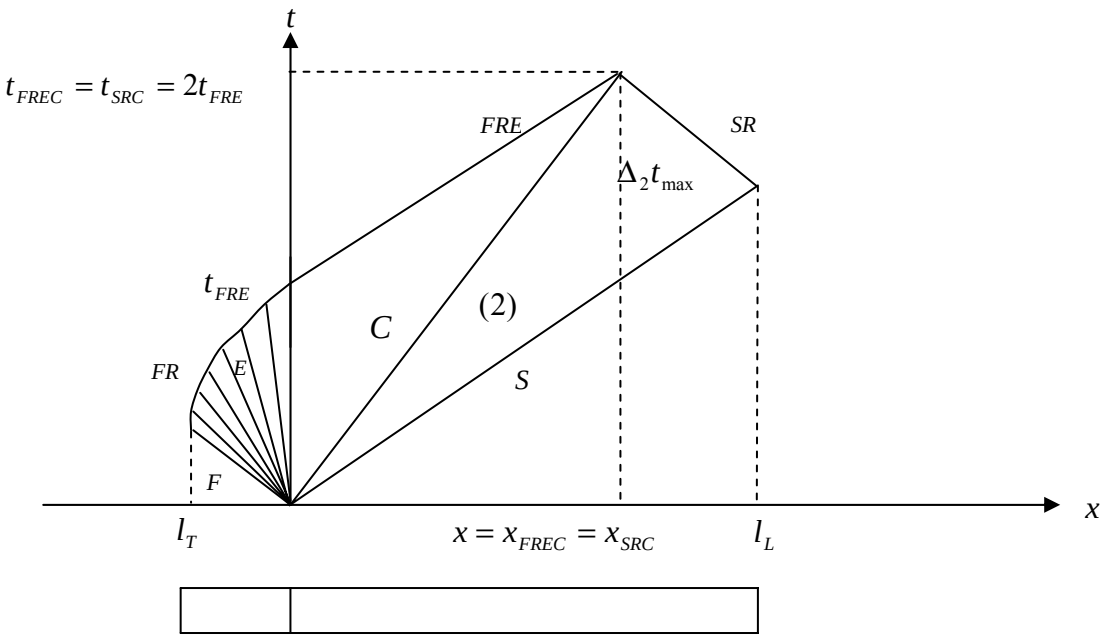

Figure 3-6 Path (x) –Time (t) –diagram in case of maximum dwell time $\Delta_2 t$ while the pressure p_2 behind the incident shock wave S maintains undisturbed. Maximum occurs where the interaction of the front of the reflected expansion wave FRE and the contact surface C and the reflected shock wave SR takes place.

With l_T as length of the drive section and l_L as length of the driven section[18], above states

$$\Delta_2 t(x_{FREC}) = \begin{cases} 2\dfrac{l_T}{a_4}\dfrac{(1+f_1)k_{21}+2(2+f_1)}{(1+f_1)[(2+f_1)+(1+f_1)k_{21}]}\cdot \\ \left(1-\dfrac{f_1 a_1}{f_4 a_4}\cdot\dfrac{k_{21}}{[(2+f_1)^2+(2+f_1)(1+f_1)k_{21}]^{\frac{1}{2}}}\right)^{-\frac{1+f_4}{2}} \end{cases} \qquad (16\text{-}17)$$

$$\Delta_2 t(x_{SRC}) = \begin{cases} \dfrac{l_L}{a_1}\left[\dfrac{(2+f_1)+(1+f_1)k_{21}}{2+f_1}\right]^{\frac{1}{2}}\cdot \\ \dfrac{(2+f_1+k_{21})[2(2+f_1)+(3+f_1)k_{21}]}{(1+k_{21})[(2+f_1)+(1+f)k_{21}]^2} \end{cases}$$

[18] Appendix A. Table A-4

In Table A-4 the relationships between quantities in Fig. 3-4 to Fig. 3-6 are given.

3.1.4.2 Tube end

The time duration between the reflected shock wave SR leaving the tube end l_L, interacting with the contact surface C and the front of the reflected expansion wave at the point x, reflecting as SRR and finally impinging into the tube end is defined as the dwell-time $\Delta_5 t$, Fig. 3-7.

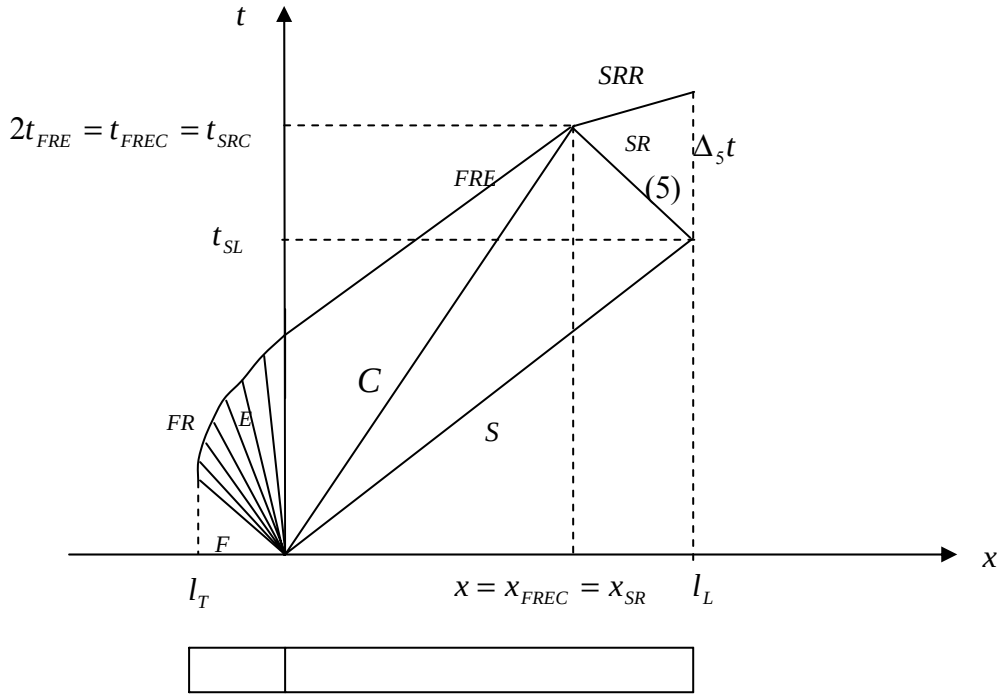

Figure 3-7 The time $\Delta_5 t$ at the point l_L while the pressure p_5 behind the reflected shock SR maintains undisturbed.

Since the determination of the tube size does not involve $\Delta_5 t$ no more investigation will be made regarding the dwell-time $\Delta_5 t$.
Though, it is possible to obtain large values of $\Delta_5 t$ with use of an adjustable medium border.[19]

3.2 Design of the shock tube

The design of the tube will be based upon the criteria of thin laminar/turbulent- or laminar-boundary layer. The reason why is to find whether or not laminar or laminar/turbulent or flow has to be taken account of in section (2) and/or (3). This will give the point where measurements will take place along the sidewall. This point will also maximize or minimize the length of the tube depending on laminar or turbulent boundary layer respective. Thereafter the

[19] [3], pp. 433-438 and pp. 456-457.

length of the tube will be decided upon the relations presented in table A-4. Also the diameter of the tube will be decided, based on the thickness of the boundary layer.

This is done disregarding the fact that there is an attenuation of the shock wave and a velocity perturbation of the shock wave and the contact surface, due to the boundary layer.
Instead, the producing of a thin laminar or turbulent boundary layer is considered.
A short summary of the works of Mirels [7] and [9] is given in App. F (Reynolds number as a transition number) and App. G (Thickness of turbulent boundary layer).

Section 3.2.1 pictures the development of thin boundary layer.
In section 3.2.2 the measure point along the sidewall is decided.
The minimum total length of the tube and length of drive/driven section is settled in section 3.2.3.
Section 3.2.4 contains criteria for the choice of diameter satisfying thin boundary layer and the diameter of the shock tube is determined.

3.2.1 Flow with thin boundary layer

The theory so far concerns ideal-flow. In practice there will be viscosity and heat-transfer effects along the sidewall of the shock tube giving birth to a boundary layer. The theory of a thin boundary layer is presented in [9]. The relevant coordinate system is fixed with respect to the wave and thereafter transformed according to [7] with respect to the wall.
Immediately after the bursting of the diaphragm, during the progress of the shock front and the expansion wave a boundary layer starts to grow at the vicinity of the sidewall, Fig. 3-8.

(a) *Shock tube before breakage of the diaphragm.*

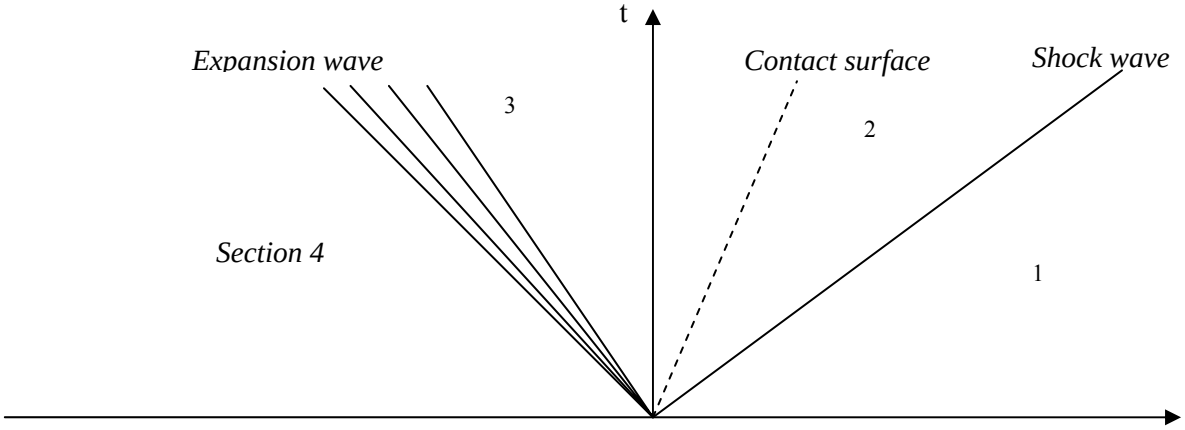

(b) *Wave diagram, ideal flow.*

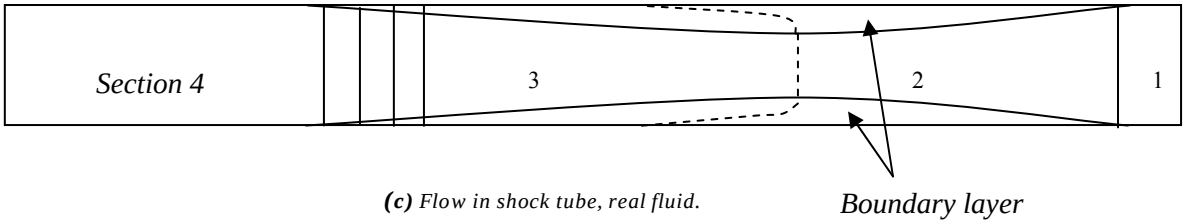

(c) *Flow in shock tube, real fluid.*

Figure 3-8 Growth of the boundary layer in a shock tube.

The boundary layer starts growing at the front of the expansion wave and the shock front and increases in thickness until it reaches a maximum at the contact surface. Section two and three are of interest. The temperature in section two is high with respect to the wall, whereas in section three the temperature is low with respect to the wall. Since the boundary layer is thin, the growth occurs in uniform unaccelerated regions. It continues growing, transition into turbulence occurs, and becomes thicker until the assumption of a zero pressure gradient in the uniform sections becomes invalid. (If this is to be the case, another theory has to be used in order to describe how the core of potential flow is affected[20]). The growth of the boundary layer in section three will take place at a higher free stream Reynolds number. The pressure gradient is assumed to be zero. Thus, the wall affects only the momentum of the fluid in the x-direction.

3.2.2 Measure point along the sidewall

Account has to be taken of whether there is primarily laminar or primarily turbulent boundary layer in each of the sections (2) and (3). Thereafter the measure point x_m along the sidewall

[20] [10].

will be decided. Let T_T denote the point with coordinates (x_T , t_T) where transition occur. Let m denote the point with coordinates (x_m , t_m) where measurements will be made.
Assume that the boundary layer at the contact surface grows as in Fig. 3-8 i.e. unaffected of wave reflections that will occur due to the tube end. This means that the boundary layer will grow as if the reflection of waves did not occur. Further, the expansion wave is assumed to be of zero-thickness i.e. an expansion shock.

The position of the probe along the sidewall experiences the undisturbed section (2) during the time $\Delta_2 t$, i.e. from the time of the shock front passing by until the arrival of the contact surface. During this time the boundary layer will be laminar near the shock front, farther from the shock front transition into turbulence occurs. There will be three cases and primarily laminar boundary layer in one or both of the sections is the goal in the first two cases.

First case: Primarily laminar boundary layer in both sections (2) and (3).
Second case: Primarily laminar boundary layer in section (3) and primarily turbulent boundary layer in section (2).
Third case: Primarily turbulent boundary layer in both sections.

These conditions and with use of a free stream Reynolds number as a transition number will give a distance x_m along the sidewall where the probe will be placed satisfying the maximum time $\Delta_2 t_{\max}$. This point m equals $x = x_{FREC} = x_{SR}$ at the time $t_{FREC} = t_{SRC} = 2t_{FRE}$.
Let the free stream Reynolds number equal $\mathrm{Re}_T = 0.5 \cdot 10^6$ [21] and use it as a transition Reynolds number in order to establish a rough estimation where transition from laminar into turbulence occurs behind the shock/expansion wave[22]. Section (2) and (3) will be treated separately. The maximum Reynolds number occurs at the contact surface. Denote x_T as the distance the contact surface has travelled when transition into turbulence occurs at the contact surface. Along the characteristic lines bd and ab there will be primarily laminar boundary layer, Fig. 3-9.

---

[21] Appendix F.
[22] With use of a transition Reynolds number and thereby make a rough estimation where transition into turbulence occurs, it would result in a discontinuity at the contact surface. According to [7] this discontinuity does not occur, the theoretical discontinuity represents a deficiency of the method. Nevertheless it is possible to treat section two and three separately.

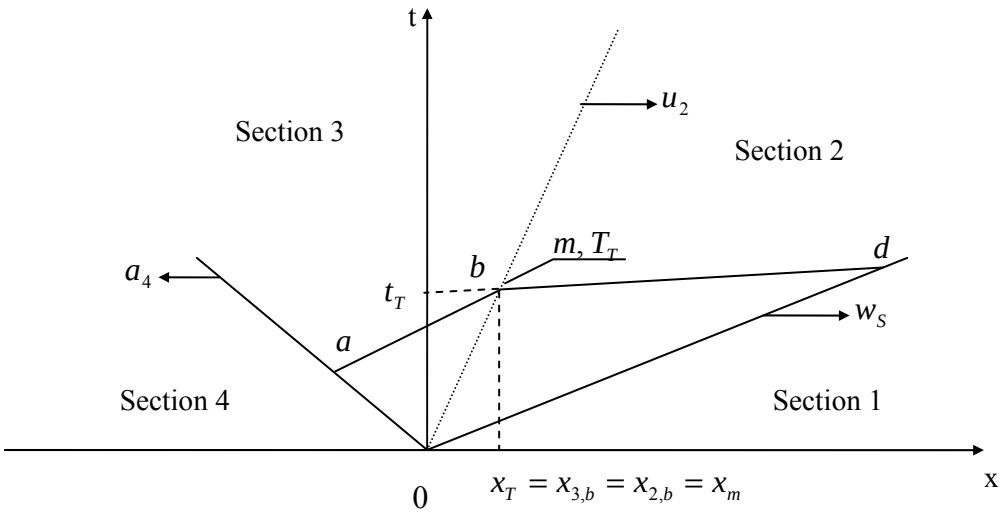

Figure 3-9 Characteristic-line geometry, ideal flow. Primarily laminar boundary layer along the characteristic lines ab and bd.

The introduced notation below is used in App. F where transition equations are derived.
Denote $\mathrm{Re}_{2,b}$ corresponding to $x_{2,b}$ and $\mathrm{Re}_{3,b}$ corresponding to $x_{3,b}$, the Reynolds number at the contact surface with respect to section (2) and section (3) respective.
Using Eqs. F.4,F.9,F.10 and H.2 the Reynolds number per meter at the contact surface are $\mathrm{Re}_{2,b}/x_{2,b}$ and $\mathrm{Re}_{3,b}/x_{3,b}$.

$$\begin{aligned} \frac{\mathrm{Re}_{2,b}}{x_{2,b}} &= a_1 \frac{\rho_2}{\rho_1}\left[\frac{\rho_1}{\mu_2}\left(\frac{u_2}{u_S}\right)\left(1+M_2-\frac{w_S}{a_2}\right)M_S\right] \\ \frac{\mathrm{Re}_{3,b}}{x_{3,b}} &= a_1 \frac{\rho_3}{\rho_1}\left[\frac{\rho_1}{\mu_3}\left(\frac{u_2}{u_S}\right)\left(1+M_2-\frac{w_S}{a_2}\right)M_S\right] \end{aligned} \qquad (18\text{-}19)$$

In Eq.19 $\frac{\rho_3}{\rho_1}=\frac{\rho_3}{\rho_2}\cdot\frac{\rho_2}{\rho_1}$ and[23]

$$\frac{\rho_3}{\rho_2}=\frac{2+f_4}{f_4}\cdot\left(\frac{a_1}{a_4}\right)^2\cdot\left(\frac{f_1}{1+f_1}\right)^2\cdot\frac{k_{21}+1}{k_{21}+(2+f_1)} \qquad (19.a)$$

Fig. 3-10 and 3-11 show the variation of Reynolds number per meter at the contact surface with respect to different initial values of the pressure p_1.

[23] Eq. 19.a was derived using [3], Eq. 12, p.422.

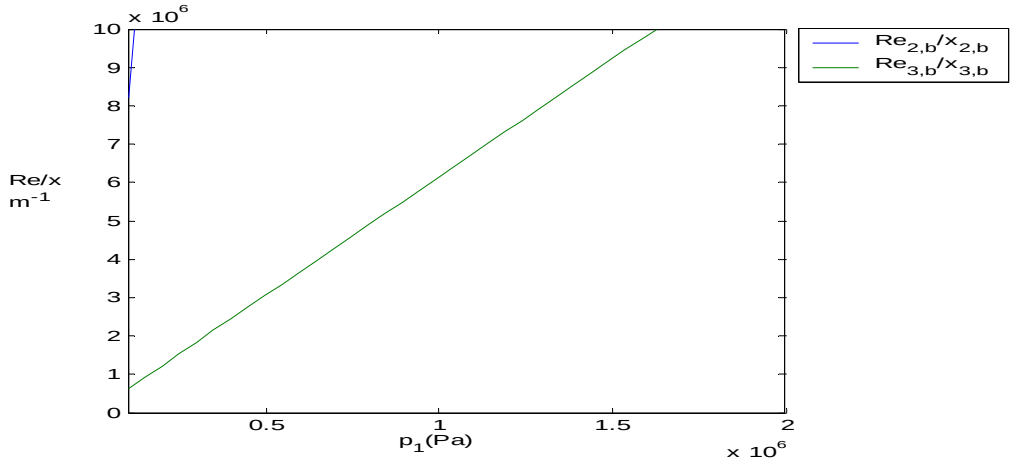

Figure 3-10 **Reynolds number per meter at contact surface with respect to different pressures p_1. Pressure range is** $100kPa \leq p_1 \leq 2MPa$.

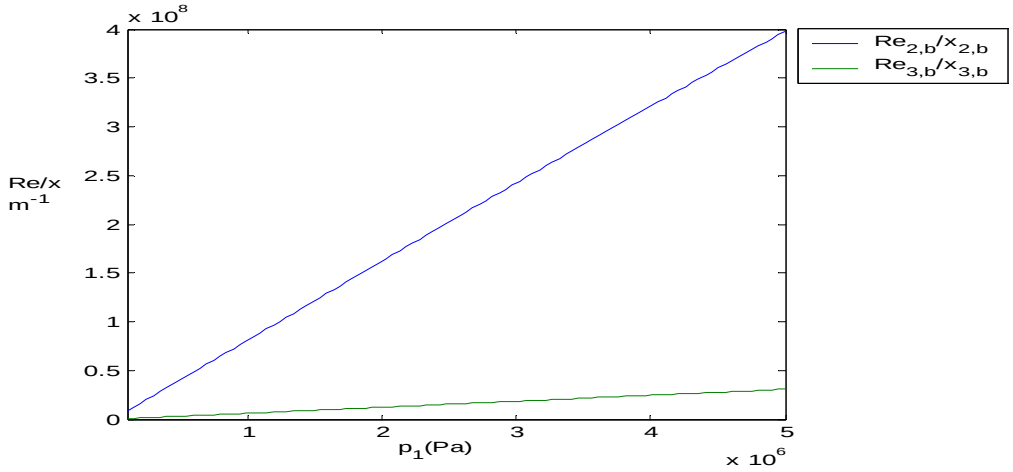

Figure 3-11 **Reynolds number per meter at contact surface with respect to different pressures p_1. Pressure range is** $100kPa \leq p_1 \leq 5MPa$.

The "worst" case is achieved when the pressure p_1 takes its highest value i.e. transition occurs earlier at higher pressure and the point x_T will then have to be placed closer to the diaphragm if we want to obtain primarily laminar boundary layer in section (2) and/or section (3).
Let $x_m = 1m.$ be the minimum length from the diaphragm where measurements will be made (to avoid disturbances from the breakage of the diaphragm).

First case: Primarily laminar boundary layer in both sections.
The conditions $\mathrm{Re}_{2,b} < \mathrm{Re}_T$ and $\mathrm{Re}_{3,b} < \mathrm{Re}_T$ imply that primarily laminar boundary layer in both sections is not attainable, see Fig. 3-10.

Second case: Primarily laminar boundary layer in section (3) and primarily turbulent boundary layer in section (2).
The condition $\mathrm{Re}_{3,b} < \mathrm{Re}_T$ implies that primarily laminar boundary layer in section (3) is not attainable, see Fig. 3-10.

Third case: Primarily turbulent boundary layer in both sections.
The conditions $\mathrm{Re}_{3,b} \geq \mathrm{Re}_T$ and $\mathrm{Re}_{2,b} \geq \mathrm{Re}_T$ imply that primarily turbulent boundary layer in both sections is attainable from approximately $p_1 = 100kPa$, see Fig. 3.10.

Only the third case is possible if the goal is to have similar boundary layer development disregarded the pressure p_1 and if so, primarily turbulent boundary layer has to be attainable from $p_1 = 100kPa$.

This arguing will result in following conditions to consider,

i) $p_1 \geq 100kPa$
ii) $\mathrm{Re}_{3,b} \geq \mathrm{Re}_T$

in order to determine the point x_m where measurements will be made. Section (3) will be treated because of $\mathrm{Re}_{3,b}/x_{3,b} < \mathrm{Re}_{2,b}/x_{2,b}$. Transition occurs for a higher value of Reynolds number in section (3) and the goal is to have primarily turbulent boundary layer in section (3) as well.

Moreover, still the boundary layer along the characteristic line ab (Fig. 3-9) is primarily laminar if $p_1 = 100kPa$ and $\mathrm{Re}_{3,b} = \mathrm{Re}_T$. Thus, x_m has to be placed a longer distance from the diaphragm, which means that nor will x_m nor x_T be placed at $x_T = x_{3,b} = x_m$, compare Fig. 3-9 with Fig 3-12.

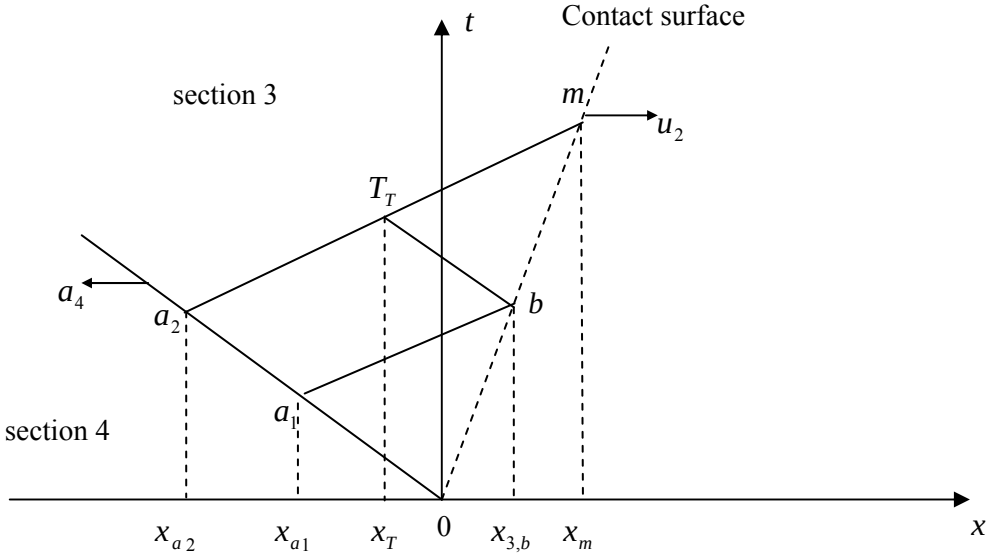

Figure 3-12 Primarily laminar boundary layer along the characteristic line a_1b and primarily turbulent bounder layer along the characteristic line a_2m. Pressure p_1 = 100kPa.

These are rough estimations and suppose that if the transition into turbulent boundary layer occurs at half of the measure time then let the boundary layer along the line a_2m to be considered as primarily turbulent, Fig.3-12. The distance $x_{3,b} - x_{a1}$ behind the expansion shock, where there is primarily laminar boundary layer, is constant. The point T_T denotes where

transition occurs. As time goes by the distance $x_m - x_{a2}$ increases until the point T_T is in the middle between the points a_2 and m. Distance relations are as follow:

$$\begin{aligned} x_T - x_{a2} &= x_{3,b} - x_{a1} \\ x_m - x_{a2} &= 2(x_{3,b} - x_{a1}) \\ x_{3,b} - x_T &= -x_{a1} \end{aligned} \tag{20}$$

The relations in Eq. 20 give

$$x_m = 2x_{3,b} \tag{21}$$

The point $x_{3,b}$ will be evaluated under the conditions $p_1 = 100kPa$ and $\mathrm{Re}_{3,b} = \mathrm{Re}_T$ using the Eqs. F.9-10 and H.4.
The point $x_m = 1.6m.$ and it is the distance from the diaphragm where measurements along the sidewall will take place. It is now reasonable to consider primarily turbulent boundary layer in both sections (2) and (3) disregarded the pressure p_1.

This is the minimum distance, placing the measure point beyond this distance still guarantee primarily turbulent boundary layer in both sections (2) and (3) disregarded the pressure p_1. The choice of $x_m = 1.6m.$ as the point for placing the measure station along the tube side will minimize the total length of the shock tube.

3.2.3 Length of the shock tube

The minimum total length of a shock tube satisfies:

i) Maximum dwell-time in section (2) ideal flow.
ii) Primarily thin turbulent boundary layer in both section (2) and (3).
iii) Combination of gases He/Ar.
iv) Measure station placed at a distance of $1.6m$ from the diaphragm.

The length of the drive/driven section is evaluated with use of equations in Table A-4.
The length of the drive section is $l_T = 2.7m$.
The length of the driven section is $l_L = 2.3m$.
The total length of the shock tube is $L = 5.0m$.

3.2.4 Diameter of the shock tube

The assumption is thin boundary layer compared to the diameter of the tube. This means that the thickness of the boundary layer has to be investigated. Only the case of primarily turbulent boundary layer in section (2) and (3) will be treated since this will be the case for all the pressures $100kPa \le p_1 \le 5MPa$. The thickness $\tilde{\delta}$ of the turbulent boundary layer[24] has its maximum at the contact surface and the case with respect to section (2) at the point m will be treated. $\tilde{\delta}$ was evaluated for different pressures p_1 with use of the Eqs. in App. G and App. H, finally with Eq. G.18. Temperature at the wall in section (2) is $T_{2,w} = T_1 = 288.15K$. In Eq. G.18, x_1 was evaluated as if the incident shock wave was propagated in a tube with a driven

[24] Appendix G.

section of the length x_1 with respect to the time t_m, i.e. no reflection of the incident shock wave. In Fig. 3-13 the thickness of turbulent boundary layer at the contact surface se is plotted against different pressures p_1 at point m.

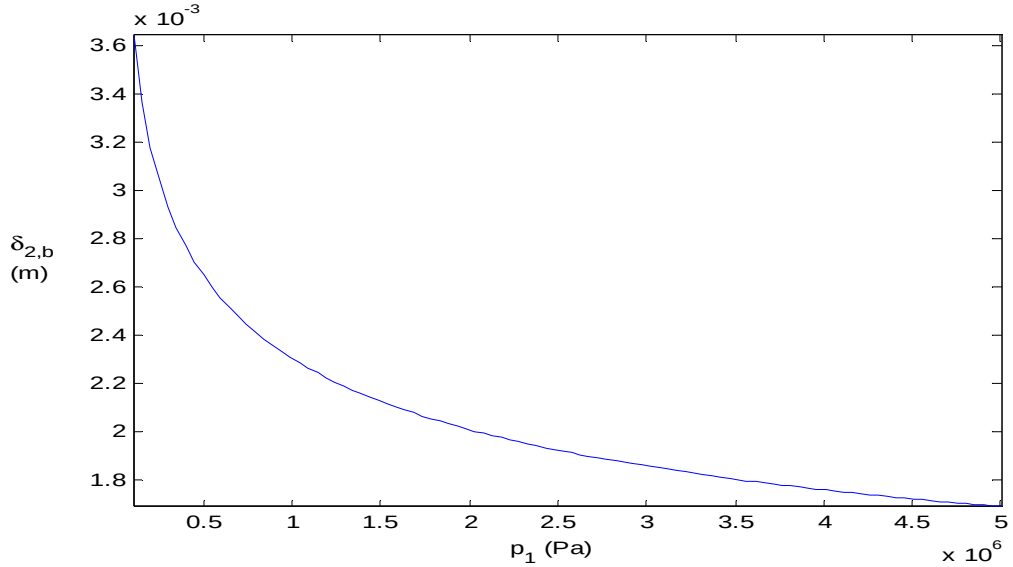

Figure 3-13 Thickness of turbulent boundary layer, with respect to different pressures p_1. Pressure range, $100kpa \leq p_1 \leq 5Mpa$.

Thickest turbulent boundary layer arises when the pressure p_1 equals $100kPa$. In lack of sufficient information the criteria for thin boundary layer with respect to the radius of the shock tube will be set at 10% of the radius.

The maximum thickness at point m is $\tilde{\delta}_m(p_1 = 100kPa) = 3.6 \cdot 10^{-3}\ m$.

The diameter of the shock tube that satisfies the criteria of thin turbulent boundary layer is at minimum $D = 0.073\ m$.

3.3 Handling of the shock tube

The driver section contains Helium and the driven section contains Argon. During the loading of gas phase the gas temperature inside shall be kept at constant temperature. Also the temperature at the tube wall shall be kept constant. This will be a rather slow process. The initial pressures needed in the drive/driven section are obtained from the characteristic functions Eq. 15 and are pictured in Fig. 3-3. A survey of the resulting pressures can be achieved by drawing a horizontal line from the known value of the proposed pressure step on the p-axis. Then, draw a vertical line from the intersection of the characteristic curve Δp_{21} or Δp_{51} covering the range of $0 - 40MPa$ along the p-axis. All the intersections (vertical line) at the characteristic functions are the resulting pressures.

4 Discussion and conclusions

This section contains discussion of the result, conclusions and suggesting future works.

4.1 Maximum length and accurate diameter of the shock tube

It was stated that the length of the tube was to be minimized. A maximum length of the shock tube may possibly be set by the investigation of a limiting separation distance.
According to Mirels and Brown [8], the boundary layer in section (3) generates longitudinal compression waves meanwhile in section (2) the generation of expansion waves occurs. The net effect is an attenuation of the shock wave. The boundary layer will modify the wave system and the flow variables, changing the properties of the flow, by the continuous generation of non-stationary compression and expansion waves due to the vertical velocity at the edge of the boundary layer. Hence, there are no uniform-flow sections. The magnitude of these effects depends mainly of the shock strength, the type of boundary layer and the cross sectional area and length of the tube. In the case of small perturbations generated by the boundary layer the theory presented in [8] may be used. The boundary layer in section (2) gives birth to a mass-sink in this section. This will cause the incident shock wave to decelerate and the contact surface to accelerate. The estimated test time in section (2) will thereby be less than in the ideal shock tube predicted. The separation distance between the incident shock wave and the contact surface attains a maximum value and has been analytically determined in [19], though low-density shock tubes. According to [5], the maximum test time and separation distance for a turbulent boundary layer depend primarily on the initial pressure p_1 and the hydraulic diameter $d \equiv 4A/l$, for a given shock Mach number. Perhaps this may be used in order to find a more accurate length and diameter of the shock tube.

4.2 Spectrum of generated signal

The spectrum of the generated signal is not discussed in this work. Account should be taken to real flow effects and there will be a deviation from the ideal step. For instance, the width of the shock front has to be investigated to determine the band width.

4.3 One-dimensional theory

According to Hubbard/Boer [15] the flow field nearly behaves as in one-dimensional theory at distances greater than a tube radius behind the shock front. However, their work is based on the work of Mirels [16], which deals with low-pressure shock tubes with the initial pressures of the order of $0.1\ kPa$. In this report the initial pressures are at least $100\ kPa$ and the wall boundary layer effects are assumed less pronounced. Further, in [15] the study was made regarding two-dimensional flow.

4.4 Thin turbulent boundary layer

The assumption of thin boundary layer is perhaps correct but turbulence eventually occurs not only in the boundary layer but also in the whole tube flow, i.e. long tubes. The boundary layer grows to a certain extend and thereafter transition into turbulent tube flow occurs. There will be a deviation from the thin boundary layer theory. Smeets and Mathieu make remarks on this in [20]. The study reflects turbulent boundary layer in high enthalpy flows. The minimum diameter

of the tube was stated in section (3.4) satisfying thin turbulent boundary layer. The point issue is the connection to small perturbation of the potential flow discussed in section 4.1.

4.5 The drag coefficient (App. G)

The drag coefficient was evaluated in [13] under the assumption of that the boundary layer on the plate is turbulent from the leading edge. Turbulence in the boundary layer in section (2) appears closely behind the incident shock wave. The effect on the thickness of the boundary layer is probably small.

4.6 Reynolds number as a transition number

Transition Reynolds numbers lower/higher than $\mathrm{Re}_T = 0.5 \cdot 10^6$ has been experimentally verified according to [16]. Higher values appear for higher values of M_S. Probably the estimation done in this report is sufficient.

4.7 Station of measurements at the tube end

High values of pressure steps occur at the tube end. Closer investigation of the behaviour of the boundary layer due to the reflection of the incident shock wave is necessary. The "tripple" point indicating the interaction of the reflected shock wave, reflected expansion wave and the contact surface, is probably only of theoretical interest. In section 4.1 stated real flow effects will probably displace the interaction either way, which means that the interaction will be one of the below:

i) Reflected shock/contact surface.
ii) Reflected expansion wave/contact surface and thereafter interacting with the reflected shock wave.

The resulting expansion/shock wave then propagates towards the tube end and finally impinges into the endwall. This will determine the dwell-time in section (5).

4.8 Alternative choice of gases

The choice of He / N_2 as combination of gases is an alternative to the choice made in this report. The pressure steps will still be obtainable. The shock strength will be taken a value close to the presented one. The dimensioning of the shock tube has to be done in the same manner as in this report.

4.9 Pressure drop

In section 4.1 stated real flow effects give rise to a pressure drop. The probes will experience a pressure drop during the test time. If account is taken to real flow effects; the characteristic functions presented in this report have to bee correlated.

4.10 Temperature

Temperature was not discussed in this report. For given f, all quantities depend only on the initial pressure p_1. In real applications probes are experienced different temperature and it is

advisable to take account of this as well. All quantities would thereby be expressed by the two variables p_1 and T_1.

4.11 Coefficient of pressure step efficiency

Depending on whether the dimensioning of the shock tube should be with respect to Δp_{21} or Δp_{51}, maximum value of $c_{e,2}$ or $c_{e,5}$ with respect to k_{21} or k_{51} perhaps may be used to determine the value of k_{21} or k_{51}.

4.12 Uncertainties

No uncertainties are discussed in this report. It is suggested to do this after the final modelling has been done which concerns the remarks made in precedent sections above.

5 Bibliography

[1] Anderson, J.D., Jr. (2003), *Modern Compressible Flow with Historical Perspective*. 3rd ed. New York: McGraw-Hill. ISBN 0-07-112161-7.

[2] Liepmann, W. & Roshko, A. (2001), *Elements of Gasdynamics*. Mineola: Dover Publications, Inc. ISBN 0-486-41963-0 (pbk).

[3] Oertel, H. (1966), *Stossrohre*. Wien: Springer-Verlag.

[4] Hjelmgren, J. (2003), *Nätverk för Dynamiska Mätningar-Behovsanalys, Kompetenshöjning och Forskningsprioritering*. SP Report 2003:27. Borås: SP Swedish National Testing and Research Institute. ISBN 91-7848-963-6.

[5] Glass, I. I. & Sislian, J. P. (1994), *Nonstationary Flows and Shock Waves*. Oxford engineering series; 39. New York: Oxford University Press Inc. ISBN 0-19-859388-0.

[6] Hjelmgren, J. (2002), *Dynamic Measurements of Pressure - A Literature Survey*. SP Report 2002:34. Borås: SP Swedish National Testing and Research Institute. ISBN 91-7848-925-3.

[7] Mirels, H. (1956), *Attenuation in a Shock Tube due to Unsteady -Boundary -Layer Action*. TN 3278. Washington: National Advisory Committee for Aeronautics.

[8] Mirels, H. & Braun, W. H. (1957), *Nonuniformities in Shock-Tube Flow due to Unsteady - Boundary -Layer Action*. TN 4021. Washington; National Advisory Committee for Aeronautics.

[9] Mirels, H. (1956), *Boundary Layer Behind Shock or Thin Expansion Wave moving into Stationary Fluid.* TN 3712. Washington; National Advisory Committee for Aeronautics.

[10] Trimpi, R. L. & Cohen, N. B. (1955), *A Theory for Predicting the Flow of Real Gases in Shock Tubes with Experimental Verification.* TN 3375. Washington; National Advisory Committee for Aeronautics.

[11] Schlichting, H. (1949), *Part I - Laminar flows.* Lecture Series "Boundary Layer Theory". TM 1217. Washington; National Advisory Committee for Aeronautics.

[12] *AGA Gashandbok* (1982), Kersti Ahlberg & Olle Lindskog (red.). Lidingö; AGA AB. ISBN 91-970061-0-6.

[13] Schlichting, H. (1949), *Part II - Turbulent flows.* Lecture Series "Boundary Layer Theory". TM 1218. Washington; National Advisory Committee for Aeronautics.

[14] Nagamatsu, H. T. (1961), Shock Tube Technology and Design. *Fundamental Data obtained from Shock-Tube Experiments*. Pergamon Press. pp 86-133.

[15] Hubbard, E. W. & de Boer P.C.T. (1970), Flow Field Behind a Shock Wave in a Low Pressure Test Gas. *Shock Tubes.* Proceedings of the Seventh International Shock Tube Symposium. Edited by I.I. Glass. Toronto; University of Toronto Press. pp. 109-125. ISBN 0-8020-1729-0.

[16] Mirels, H. (1963), Test Time in Low-Pressure Shock Tubes. *The Physics of Fluids*. Volume 6, pp. 1201-14.

[17] Lacey, J. J., Jr. (1970), Experimental Shock Tube Test Time - Turbulent Regime. *Shock Tubes.* Proceedings of the Seventh International Shock Tube Symposium. Edited by I.I. Glass. Toronto; University of Toronto Press. pp. 126-142. ISBN 0-8020-1729-0.

[18] Hertzberg, A. (1970), Shock Tube Research, Past, Present and Future: A Critical Survey. *Shock Tubes.* Proceedings of the Seventh International Shock Tube Symposium. Edited by I.I. Glass. Toronto; University of Toronto Press. pp. 3-5. ISBN 0-8020-1729-0.

[19] Mirels, H. (1966), Flow Nonuniformity in Shock Tubes Operating at Maximum Test Times. *The Physics of Fluids*. Volume 9, pp. 1907-12.

[20] Smeets, G. & Mathieu, G. (1988), Investigation of Turbulent Boundary Layers and Turbulence in Shock Tubes by Means of Laser Doppler Velocimetry. *Shock Tubes and Waves.* Proceedings of the 16th International Symposium on Shock Tubes and Waves. Edited by H. Grönig. VCH Verlagsgesellschaft.pp. 193-200. ISBN 3-527-26874-X.

Appendix A. Basic theory and tables

A summary is given of the theories in [1],[3] and [5].
In the first chapter the basic equations of fluid motion and thermodynamic relations are stated. Wave properties are discussed in chapter two.

A.1 Basic equations of fluid motion and thermodynamic relations

Fundamental physical principles are

a. Mass and energy is conserved.
b. Newton's second law, Force = mass x acceleration.

Together with a Finite Control Volume Approach and an Infinitesimal Fluid Element Approach[25] and for inviscid flows the basic equations of fluid motion are

Continuity equation:

$$-\oiint_S \rho\vec{V}\cdot d\vec{S} = \frac{\partial}{\partial t}\iiint_V \rho dV \tag{A.1}$$

representing the net mass flow into a control volume across the control surface, L.H.S and the increase of mass inside a control volume, R.H.S. It shows that mass is conserved. ρ is the density and $\vec{V}$ is the fluid velocity.

Momentum equation:

$$\oiint_S (\rho\vec{V}\cdot d\vec{S})\vec{V} + \iiint_V \frac{\partial(\rho\vec{V})}{\partial t} dV = \iiint_V \rho\vec{f}_b dV - \oiint_S p d\vec{S} \tag{A.2}$$

This is the integral formulation of Newton's second law. $\vec{f}_b$ is the body force per unit mass of fluid inside the control volume. p is the pressure acting on the surface from the outside of the control volume. The R.H.S. is the total force acting on the control volume. The L.H.S. of Eq.A.1 brings a momentum flow across the control surface, towards the control volume gives positive sign, and this is the first term in Eq. A.2, L.H.S. The second term is the time rate of change of momentum inside the control volume. In Eq. A.2 the effects of friction is omitted.

Energy equation:

$$\begin{aligned}&\iiint_V \dot{q}\rho dV - \oiint_S p\vec{V}\cdot d\vec{S} + \iiint_V \rho(\vec{f}_b\cdot\vec{V})dV = \\ &\iiint_V \frac{\partial}{\partial t}[\rho(e+\frac{V^2}{2})]dV + \oiint_S \rho(e+\frac{V^2}{2})\vec{V}\cdot d\vec{S}\end{aligned} \tag{A.3}$$

states that energy is conserved. $\dot{q}$ is the rate of heat added per unit mass and e is the internal energy per unit mass.
L.H.S: The first term is the rate of heat added to the fluid inside the control volume from the surroundings. The fluid inside the control volume experiences pressure forces acting on the surface from the outside of the control volume and the second term is the rate of work done on

---

[25] [1], pp.43-53.

the fluid. Also body forces acting on the fluid inside the control volume. The rate of work done due to body forces is the third term. The second and the third term represent the total work done. R.H.S: The energy per unit mass of the fluid inside moving through the control volume contains both the internal energy and the kinetic energy. Its contribution comes from the mass flow. The second term is the net rate of flow of energy across the control surface. The first term adds the time dependent change of energy that will arise due to local transient fluctuation of the flowfield and its variables.
In Eq.A.3 the phenomena of thermal conduction, diffusion and work done by viscous stress and shaft work are omitted.

Furthermore, for a thermal and calorically perfect gas (constant c_p and c_v),

Ratio of specific heats:

$$\gamma \equiv \frac{c_p}{c_v} \tag{A.4}$$

Equation of state:

$$p = \rho \frac{R_0}{A_r} T = \rho R T \tag{A.5}$$

where R_0 is the universal gas constant and A_r is the relative atomic mass.

The thermodynamic relations are,

Internal energy:

$$e = c_v T \tag{A.6}$$

Enthalpy:

$$h = e + p\upsilon \tag{A.7}$$

$$h = c_p T \tag{A.8}$$

Entropic equation of state[26]:

$$p = \frac{p_0}{\rho_0^{\gamma}} \exp[(s - s_0)/c_v]\rho^{\gamma} \tag{A.9}$$

where s is the specific entropy and subscript 0 denotes a reference state.

For an isentropic process $\Delta s = 0$ (both adiabatic and reversible) and isentropic relations are

$$\frac{a}{a_i} = \left(\frac{T}{T_i}\right)^{\frac{1}{2}} = \left(\frac{\rho}{\rho_i}\right)^{\frac{1}{f}} = \left(\frac{p}{p_i}\right)^{\frac{1}{2+f}} \tag{A.10}$$

$i = 1$ or $i = 4$. For a molecule with one or two atoms the number of degrees of freedom, $f = \frac{2}{\gamma - 1}$.

---

[26] [5], p.39

A.2 Wave properties

Subjects that are included in the chapter wave properties.
In the first section finite waves is discussed and in the second section the shock wave is discussed.
Section three deals with an incident shock wave impinging into a solid wall and thereby reflects.
Section four contains characteristics of waves.
Centred expansion wave is explained in section five.
Finally, section six deals with the properties behind an incident expansion wave impinging into a solid wall and thereby reflects.

A.2.1 Finite waves

Travelling waves that introduce large perturbations from ambient conditions are called finite waves. The local speed of sound a varies through the wave and the local mass-motion velocity u may be positive or negative. If the portion of a wave causes the increase of the density then it will be called a finite compression region. On contrary if the portion of a wave causes the decrease of the density then it will be called an expansion region. Each local part of the wave will be propagating at the local velocity $u + a$. That is relative to the laboratory and it is the local speed of sound superimposed on top of the local mass motion. A shock wave is created by a series of finite compression waves where the tail of the compression wave moves faster than the head. Finally they all coalesce into the incident shock wave. In an expansion wave the head of the wave moves faster than the tail which means that an expansion wave disperses.

A.2.2 Shock wave

For a one-dimensional approach, consider a stationary normal shock wave and gas in uniform motion across the shock wave and the relationship between conditions ahead of the shock wave and behind, as stated in Fig A-1.

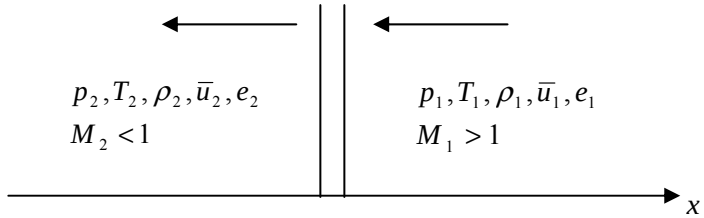

Figure A-1 Gas in uniform motion cross a stationary normal shock wave.

Here the pressure, temperature, density, flowfield velocity, and internal energy are denoted p, T, ρ, u and e respectively and the flow properties change with respect to x , as the gas flows through the region. Assume steady flow and that viscous and diabetic effects act within the transition front only. The regions on both side of the shock wave can then be considered as one-dimensional isentropic states. The equations obtained in App. A.1. are reduced to

$$\begin{aligned} \rho_1 \bar{u}_1 &= \rho_2 \bar{u}_2 \\ p_1 + \rho_1 \bar{u}_1^{\,2} &= p_2 + \rho_2 \bar{u}_2^{\,2} \\ h_1 + \frac{1}{2}\bar{u}_1^{\,2} &= h_2 + \frac{1}{2}\bar{u}_2^{\,2} \end{aligned} \qquad \text{(A.11-13)}$$

Eq. A.13 relates conditions at two equilibrium states and of the flow. Eq. A.12 holds for steady flow in a duct of constant area. Regarding a shock-wave formation, it is sufficient to calculate

the jump in the equilibrium values and to represent the shock as a discontinuity. Thus, hold on to adiabatic flow and the change in entropy $\Delta s > 0$ across the shock wave. These equations are valid for gas velocities relative to the shockwave. The speed of sound a can be interpreted as the speed at which small disturbances are propagated through a compressible fluid. Keeping with isentropic process inside a sound wave, for a perfect gas with A_r as relative atomic mass,

$$a^2 = \frac{\gamma p}{\rho} = \gamma \frac{R_0}{A_r} T \tag{A.14}$$

and define the Mach number

$$M \equiv \frac{u}{a} \tag{A.15}$$

A moving normal shock wave with velocity w_S moving into section (1) is pictured in Fig A-2. The gas in section (1) is now stagnant. During the process the propagating shock wave induces the gas in section (2) to move with a mass motion u_p, Fig A-2.

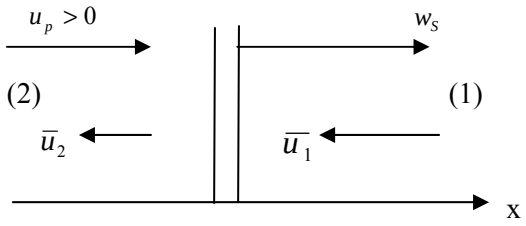

Figure A-2 Moving shock wave into a stagnant gas.

Let w_S equals the velocity of the gas ahead of the shock wave and $w_S - u_p$ equals the velocity of the gas behind the shock wave, relative to the wave.
Fig. A-2 results in $\bar{u}_1 = -w_S$ and $\bar{u}_2 = u_p - w_S$. Eqs. A.11 through A.13 become

$$\begin{aligned} \rho_1 w_S &= \rho_2 (w_S - u_p) \\ p_1 + \rho_1 {w_S}^2 &= p_2 + \rho_2 (w_S - u_p)^2 \\ h_1 + \frac{1}{2} {w_S}^2 &= h_2 + \frac{1}{2} (w_S - u_p)^2 \end{aligned} \tag{A.16-18}$$

They are the normal-shock wave equations describing the process in Fig. A.2. and they are valid for a shock wave moving with velocity w_S into a stagnant gas.
Using of Eqs. A.16 through A.18 and using A.7, giving the *Hugoniot equation:*

$$e_2 - e_1 = \frac{(p_1 + p_2)}{2} \left(\frac{1}{\rho_1} - \frac{1}{\rho_2} \right) \tag{A.19}$$

It relates thermodynamic quantities across a normal shock wave whether or not the shock wave is moving. Let the moving shock Mach number $M_S = w_S / a_1$ where a_1 is the velocity of sound in section (1), Fig. A-2. Using of Eqs. A.14 through A.18 relationships between sections (2) and (1) may be derived.

In table A-1 and A-2 there are several relationships between sections (2) and (1) presented and M_S can be expressed as

$$M_S = \sqrt{\frac{1 + f_1}{2 + f_1} \left(\frac{p_2}{p_1} - 1 \right) + 1} \tag{A.20}$$

The local mass motion induced behind the propagating shock wave can be expressed as

$$u_p = u_2 = f_1 a_1 \frac{M_S{}^2 - 1}{M_S(f_1 + 1)} \tag{A.21}$$

A.2.3 Reflected shock wave

Consider an incident normal shock wave impinging into a flat end wall creating a reflected normal shock wave as shown in Fig A-3.

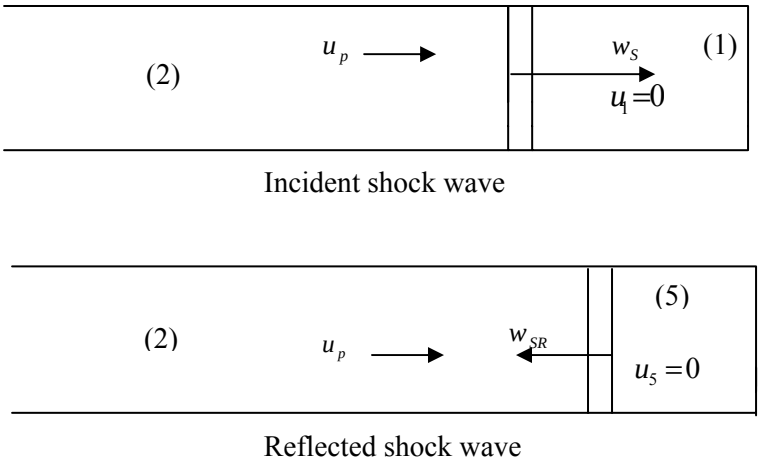

Figure A-3 Incident shock wave and reflected shock wave.

It's necessary to impose the boundary condition $u_5 = 0$ because of the solid end wall.

Denote w_{SR} as velocity of the gas behind the shock wave relative to the wave.

Let $w_{SR} + u_p$ denote the velocity of the gas ahead of the shock wave relative to the wave.

With use of Eqs A.11 through A.13 continuity, momentum and energy equations for a normal reflected shock wave become

$$\begin{aligned} \rho_2(w_{SR} + u_p) &= \rho_5 w_{SR} \\ p_2 + \rho_2(w_{SR} + u_p)^2 &= p_5 + \rho_5 w_{SR}{}^2 \\ h_2 + \frac{1}{2}(w_{SR} + u_p)^2 &= h_5 + \frac{1}{2} w_{SR}{}^2 \end{aligned} \tag{A.22-A.24}$$

Using of Eqs. A.16 through A.18 and Eqs. A.22 through A.24 gives the relationship between incident and reflected shock

$$\begin{aligned} \frac{\rho_5 - \rho_2}{\rho_2 - \rho_1} &= \frac{w_S}{w_{SR}} & \frac{\rho_5 - \rho_1}{\rho_2 - \rho_1} &= 1 + \frac{w_S}{w_{SR}} \\ \frac{p_5 - p_2}{p_2 - p_1} &= \frac{\rho_5 w_{SR}}{\rho_1 w_S} & \frac{p_5 - p_1}{p_2 - p_1} &= \frac{\rho_2}{\rho_1}\left(1 + \frac{w_{SR}}{w_S}\right) \\ \frac{h_5 - h_2}{h_2 - h_1} &= \frac{\rho_5 w_{SR}}{(\rho_2 + \rho_1) w_S} & \frac{h_5 - h_1}{h_2 - h_1} &= 2\frac{1 + \frac{w_{SR}}{w_S}}{1 + \frac{\rho_2}{\rho_1}} \end{aligned} \tag{A.25-27}$$

Introduce $M_{SR} = (w_{SR} + u_p)/a_2$ and express M_{SR} as a function of M_S:

$$M_{SR} = \sqrt{\frac{(2+f)M_S{}^2 - 1}{M_S{}^2 + f}} \tag{A.28}$$

Table A-3 lists relations between incident and reflected shock wave.

A.2.4 Characteristics of waves

The differential form of the continuity equation is

$$\frac{\partial \rho}{\partial t} + \vec{\nabla} \cdot (\rho \vec{V}) = 0 \tag{A.29}$$

Define the substantial derivative:

$$\frac{D}{Dt} \equiv \frac{\partial}{\partial t} + (\vec{V} \cdot \vec{\nabla}) \tag{A.30}$$

as the instantaneous time rate of a quantity of a given fluid element as it moves through space.

Eq. A.30 into A.29 yields:

$$\frac{D\rho}{Dt} + \rho \vec{\nabla} \cdot \vec{V} = 0 \tag{A.31}$$

and it states that the mass of a fluid element is constant as it moves through space.

The momentum equation can be written as

$$\rho \frac{D\vec{V}}{Dt} = -\vec{\nabla} p + \rho \vec{f}_b \tag{A.32}$$

In case of one-dimensional isentropic flow, constant cross-section area and no body force acting, Eqs. A.31 and A.32 become

$$\begin{aligned} \frac{1}{a^2}\left(\frac{\partial p}{\partial t} + u\frac{\partial \rho}{\partial x}\right) + \rho \frac{\partial u}{\partial x} &= 0 \\ \frac{\partial u}{\partial t} + u\frac{\partial u}{\partial x} + \frac{1}{\rho}\frac{\partial p}{\partial x} &= 0 \end{aligned} \tag{A.33-34}$$

Adding and subtracting Eqs. A.33 and A.34,

$$\left[\frac{\partial u}{\partial t} + (u \pm a)\frac{\partial u}{\partial x}\right] + \frac{1}{\rho a}\left[\frac{\partial p}{\partial t} + (u \pm a)\frac{\partial p}{\partial x}\right] = 0 \tag{A.35}$$

The paths satisfying the equations

$$\frac{dx}{dt} = u \pm a = const. \tag{A.36}$$

are called the characteristic curves. Let δ denote the differential along the characteristic curves where δu, δp and $\delta \rho$ (changes corresponding to dt and dx) are constrained to move along and

$$\delta u \pm \frac{\delta p}{\rho a} = 0 \quad \text{or} \quad \delta u \pm \frac{a}{\rho}\delta \rho = 0 \tag{A.37}$$

along characteristic curves for a calorically perfect gas.

Combining the energy and continuity equation give

$$\frac{dx}{dt} = u = const. \tag{A.38}$$

representing particle paths.

Eq. A.37 may be integrated[27] and along characteristic curves and for a calorically perfect gas the Riemann invariants are

$$J_{\pm} = u \pm fa \tag{A.39}$$

and they are constant along characteristic curves.

A.2.5 Centred expansion wave

In case of a left-running centred expansion wave there are left-running characteristics that originate from the origin. Added to these, right-running characteristics that originate from the constant property of section (4), Fig. A-4.

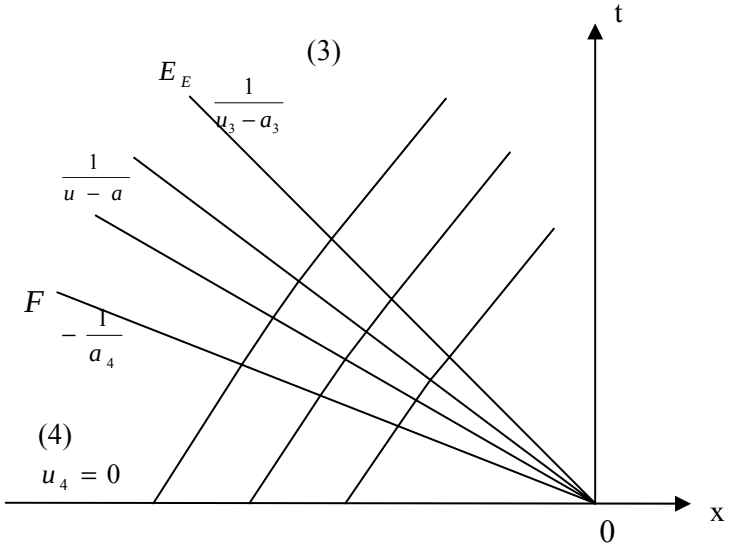

Figure A-4 Characteristics for a left-running centred expansion wave.

F is the front of the expansion wave and E_E is the tail of the expansion wave.
The Riemanns invariants are constant through the expansion wave on each of the characteristic curve. For left-running characteristics through the origin,

$$\frac{x}{t} = u - a \tag{A.40}$$

Moreover, in section (4)

$$fa + u = f_4 a_4 + u_4 = f_4 a_4 = \text{const.} \tag{A.41}$$

From Eqs. A.40 and A.41 follow

---

[27] [3], p.207.

$$\begin{aligned} a &= \frac{f_4}{1+f_4}(a_4 - \frac{1}{f_4}\cdot\frac{x}{t}) \\ u &= \frac{f_4}{1+f_4}(a_4 + \frac{x}{t}) \end{aligned} \qquad \text{(A.42-43)}$$

and Eq. A.39 for J_+ and A.41 give

$$\frac{a}{a_4} = 1 - \frac{1}{f_4}\left(\frac{u}{a_4}\right) \qquad \text{(A.44)}$$

With use of Eqs. A.10 and A.44 the properties between section (3) and (4) can be derived as a function of the local gas velocity. Eq. A.43 into Eq. A.44 and with Eq. A.10, give the variation of properties in a centred expansion wave between the head and the tail of the expansion waves as a function of x and t and $-a_4 \le x/t \le u_3 - a_3$. Table A-5 contains derived expressions.
The pressure properties obtained by a centred expansion wave as a function of the local gas velocity, can be written as

$$\frac{p_3}{p_4} = \left[1 - \frac{1}{f_4}\left(\frac{u_3}{a_4}\right)\right]^{2+f_4} \qquad \text{(A.45)}$$

Solving for the local gas velocity

$$u_3 = f_4 a_4\left[1 - \left(\frac{p_3}{p_4}\right)\right]^{\frac{1}{2+f_4}} \qquad \text{(A.46)}$$

A.2.6 Reflected expansion wave

The sections that are mentioned refer to notation used in Fig. 2-7. The properties behind the reflected expansion wave may be derived as follows.
For a left-running characteristic, between (6) and (3) holds the relation

$$u_3 - f_4 a_3 = u_6 - f_4 a_6 \qquad \text{(A.47)}$$

For a right-running characteristic, between (4) and (3) holds the relation

$$u_3 + f_4 a_3 = u_4 + f_4 a_4 \qquad \text{(A.48)}$$

The boundary conditions are $u_4 = u_6 = 0$ and subtraction of the two equations yields

$$\frac{a_6}{a_4} = 2\frac{a_3}{a_4} - 1 \qquad \text{(A.49)}$$

The change of states in case of the reflected expansion wave is considered to be isentropic and by use of Eq. A.10

$$2\left(\frac{p_3}{p_4}\right)^{\frac{1}{2+f_4}} - 1 = \left(\frac{T_6}{T_4}\right)^{\frac{1}{2}} = \left(\frac{\rho_6}{\rho_4}\right)^{\frac{1}{f_4}} = \left(\frac{p_6}{p_4}\right)^{\frac{1}{2+f_4}} \qquad \text{(A.50)}$$

Solving for the ratio p_6 / p_1 and $p_2 = p_3$

$$\frac{p_6}{p_1} = \frac{p_4}{p_1}\left[2\left(\frac{p_2}{p_4}\right)^{\frac{1}{2+f_4}} - 1\right]^{2+f_4} \tag{A.51}$$

A.3 Tables

Listed equations containing the pressure strength k_{21} are derived from equations stated in [3]. k_{21} refers to definition made in section 3.1.1. For a molecule with one or two atoms, the number of degrees of freedom $f = \frac{2}{\gamma - 1}$.

Table A-1 Changes in status across a shock wave perfect gases.

Variable	$\frac{\rho_2}{\rho_1}$	$\frac{p_2}{p_1}$	k_{21}
$\frac{p_2}{p_1}$	$\frac{(1+f)\frac{\rho_2}{\rho_1} - 1}{(1+f) - \frac{\rho_2}{\rho_1}}$	$\frac{p_2}{p_1}$	$k_{21} + 1$
$\frac{\rho_2}{\rho_1}$	$\frac{\rho_2}{\rho_1}$	$\frac{1 + (1+f)\frac{p_2}{p_1}}{(1+f) + \frac{p_2}{p_1}}$	$\frac{(1+f)k_{21} + (2+f)}{k_{21} + (2+f)}$
$\frac{T_2}{T_1} = \left(\frac{a_2}{a_1}\right)^2$	$\frac{(1+f)\frac{\rho_2}{\rho_1} - 1}{\frac{\rho_2}{\rho_1}(1+f-\frac{\rho_2}{\rho_1})}$	$\frac{\frac{p_2}{p_1}(1+f+\frac{p_2}{p_1})}{1+(1+f)\frac{p_2}{p_1}}$	$\frac{(k_{21}+1)[k_{21}+(2+f)]}{(1+f)k_{21}+(2+f)}$

Table A-2 Relations behind a moving normal shock perfect gases.

Variable	k_{21}
$\frac{u_2}{w_S}$	$\frac{f\,k_{21}}{(2+f)+(1+f)k_{21}}$
$M_2 = \frac{u_2}{a_2}$	$\frac{f\,k_{21}}{[k_{21}+(2+f)]^{\frac{1}{2}}[(k_{21}+1)(2+f)]^{\frac{1}{2}}}$

Table A-3 Relations between incident and reflected shock wave.

Variable	k_{21}
$\frac{w_{SR}}{w_S}$	$\frac{2k_{21}+(2+f)}{(1+f)k_{21}+(2+f)}$
$\frac{p_5}{p_2}$	$\frac{(3+f)k_{21}+(2+f)}{(2+f)+k_{21}}$
$\frac{T_5}{T_2}=\left(\frac{a_5}{a_2}\right)^2$	$\frac{(2+f+2k_{21})[(2+f)+(3+f)k_{21}]}{(2+f)(1+k_{21})[(2+f)+k_{21}]}$

Table A-4 Relations between quantities in Fig. 2-1 and 2-2

Quantity	f = constant
$u_{EE} = u_3 - a_3$	$a_4 \dfrac{f_4(M_3 - 1)}{M_3 + f_4}$
$u_{FRE} = u_3 + a_3$	$a_4 \dfrac{f_4(M_3 + 1)}{M_3 + f_4}$
$u_p = u_2 = u_3$	$a_1 \dfrac{f_1 k_{21}}{[(2+f_1)^2 + (2+f_1)(1+f_1)k_{21}]^{\frac{1}{2}}}$
$\dfrac{a_1 t_{SRC}}{l_L}$	$\dfrac{(3+f_1)k_{21} + 2(2+f_1)}{(1+k_{21})[(2+f_1)^2 + (2+f_1)(1+f_1)k_{21}]^{\frac{1}{2}}}$
$\dfrac{x_{SRC}}{l_L}$	$\dfrac{f_1[(3+f_1)k_{21} + 2(2+f_1)]k_{21}}{(2+f_1)(1+k_{21})[(2+f_1) + (1+f_1)k_{21}]}$
$\dfrac{a_4 t_{FRE}}{l_T}$	$(1 + \dfrac{M_3}{f_4})^{\frac{1+f_4}{2}}$
$\dfrac{a_4 t_{FREC}}{l_T}$	$2\ (1 + \dfrac{M_3}{f_4})^{\frac{1+f_4}{2}}$
$\dfrac{x_{FREC}}{l_T}$	$2M_3\ (1 + \dfrac{M_3}{f_4})^{\frac{f_4-1}{2}}$
$\dfrac{a_4 \Delta_2 t}{l_T}(x_{FREC})$	$2\dfrac{(1+f_1)k_{21} + 2(2+f_1)}{(1+f_1)[(2+f_1) + (1+f_1)k_{21}]} \cdot \left(1 - \dfrac{f_1 a_1}{f_4 a_4} \cdot \dfrac{k_{21}}{[(2+f_1)^2 + (2+f_1)(1+f_1)k_{21}]^{\frac{1}{2}}}\right)^{-\frac{1+f_4}{2}}$
$\dfrac{a_1 \Delta_2 t}{l_L}(x_{SRC})$	$\left[\dfrac{(2+f_1) + (1+f_1)k_{21}}{2+f_1}\right]^{\frac{1}{2}} \cdot \dfrac{(2+f_1+k_{21})[2(2+f_1) + (3+f_1)k_{21}]}{(1+k_{21})[(2+f_1) + (1+f)k_{21}]^2}$

Table A-5 Properties behind a centred expansion wave perfect gases.

Variable	$\frac{p_3}{p_4}$	$M_3 = \frac{u_3}{a_3}$	$\frac{x}{t}$
$\frac{p_3}{p_4}$	$\frac{p_3}{p_4}$	$\left(1+\frac{M_3}{f_4}\right)^{-(2+f_4)}$	$\left[1-\frac{1}{a_4(1+f_4)}\left(a_4+\frac{x}{t}\right)\right]^{2+f_4}$
$\frac{\rho_3}{\rho_4}$	$\left(\frac{p_3}{p_4}\right)^{\frac{f_4}{2+f_4}}$	$\left(1+\frac{M_3}{f_4}\right)^{-f_4}$	$\left[1-\frac{1}{a_4(1+f_4)}\left(a_4+\frac{x}{t}\right)\right]^{f_4}$
$\frac{T_3}{T_4}$	$\left(\frac{p_3}{p_4}\right)^{\frac{2}{2+f_4}}$	$\left(1+\frac{M_3}{f_4}\right)^{-2}$	$\left[1-\frac{1}{a_4(1+f_4)}\left(a_4+\frac{x}{t}\right)\right]^{2}$
M_3	$f_4\left[\left(\frac{p_3}{p_4}\right)^{-\frac{1}{2+f_4}}-1\right]$	M_3	$f_4\frac{\left(a_4+\frac{x}{t}\right)}{\left(f_4a_4-\frac{x}{t}\right)}$

Since $p_3 = p_2$ at contact surface and using Eqs. A.20, 3 and 10, M_3 can be written as

$$M_3 = f_4\left[\frac{(2+f_1)}{k_{21}}\cdot\frac{f_4a_4}{f_1a_1}\cdot\left(\frac{(1+f_1)}{(2+f_1)}k_{21}+1\right)^{\frac{1}{2}}-1\right]^{-1} \tag{A.52}$$

Appendix B. Symbols

A	cross-sectional area of tube
A_r	relative atomic mass
$\widetilde{A}, \widetilde{B}, \widetilde{C}$	functions of f defined by Eq. 12.a
a	speed of sound
$\widetilde{b}, \widetilde{c}$	functions defined by Eqs. G.11
C	contact surface
$c_{e,i}$	coefficient of differential-pressure efficiency, $c_{e,i} = \dfrac{k_{i,j}}{p_4 / p_1}$
c_p	specific heat of constant pressure
c_v	specific heat of constant volume
D	diameter of shocktube
d	hydraulic diameter
E	expansion wave
E_E	end of expansion wave
ER	reflected expansion wave
e	internal energy per unit mass
F	front of expansion wave
FR	front of reflected expansion wave
FRE	result of FR coincides with E_E
$FREC$	FRE overtakes C
f	number of degrees of freedom, for molecule with one or two atoms $f = \dfrac{2}{\gamma - 1}$
f_b	body force per unit mass of fluid
G	function defined by Eq. G.18a
h	enthalpy
$I_{2,N}$	integral defined by Eq. G.18c, N = 6,7 or 8.
$J_{\pm}$	Riemann invariants
k_h	coefficient of heat conductivity
$k_{i,j}$	shock strength, $k_{i,j} = \dfrac{\Delta p_{i,j}}{p_j}$
L	total length of shock tube
l_T	length of the drive section of shock tube
l_L	length of the driven section of shock tube
l	perimeter of shock tube cross section
M	Mach number
m	measure point
p	pressure, (Pa)
$\dot{q}$	rate of heat added per unit mass
R	gas constant per unit mass
R_0	universal gas constant
Re	Reynolds number

$\mathrm{Re}_{2,b}$	Reynolds number at point b of section (2)
$\mathrm{Re}_{3,b}$	Reynolds number at point b of section (3)
Re_T	transition Reynolds number
S	shock wave
SR	reflected shock wave
SRR	result of SR interacting with C
s	specific entropy
T	temperature, $^\circ K$
T_T	transition point of section (3)
t	time
u, v	velocities parallel to x, y coordinates
$\bar{u}, \bar{v}$	velocities parallel to $\bar{x}, \bar{y}$ coordinates
$\vec{V}$	fluid velocity
w	velocity of shock waves
x, y	coordinates stationary with respect to wall
$\bar{x}, \bar{y}$	coordinates stationary with respect to wave
Δp	pressure step
Δs	change in entropy
$\Delta_2 t$	dwell-time of section (2)
$\Delta_5 t$	dwell-time of section (5)
$\tilde{\delta}$	fluid velocity-boundary-layer thickness, (Polhausen viewpoint)
$\bar{\delta}$	distance from the wall
δ^*	fluid boundary-layer displacement thickness, $\int_0^\infty (1 - \frac{\rho\bar{u}}{\rho_e \bar{u}_e}) d\bar{y}$
δ	differential along characteristic curve
φ	function defined by Eq. G.15
γ	ratio of specific heats
μ	coefficient of viscosity
θ	fluid boundary-layer momentum thickness, $\int_0^\infty \frac{\rho\bar{u}}{\rho_e \bar{u}_e} (1 - \frac{\bar{u}}{\bar{u}_e}) d\bar{y}$
ρ	density
σ	Prandtl number
τ	integration variable representing t
$\tilde{\tau}$	wall shear stress
υ	kinematic coefficient of viscosity
ξ	integration variable representing x
ζ_T	similarity parameter for integral solution of turbulence case, $\frac{\bar{y}}{\tilde{\delta}}$

Appendix C. Initial pressure p_1 as a variable

For given f and constant k_{21} all quantities will solely depend on the initial pressure p_1.
Let $T = T_1 = T_4 = 288.15K$.

$$k_{21} = \frac{\Delta p_{21}}{p_1} \tag{C.1}$$

$$M_S = \sqrt{\frac{1+f_1}{2+f_1} \cdot k_{21} + 1} \tag{C.2}$$

$$k_{51} = \frac{\Delta p_{51}}{p_1} = \left[\frac{(1+k_{21})[(2+f_1)+(3+f_1)k_{21}]}{k_{21}+(2+f_1)} \right] - 1 \tag{C.3}$$

$$p_2(p_1) = \Delta p_{21}(p_1) + p_1 = (k_{21}+1)\,p_1 \tag{C.4}$$

$$p_5(p_1) = \Delta p_{51}(p_1) + p_1 = (k_{51}+1)\,p_1 \tag{C.5}$$

$$p_4(p_1) = p_1(k_{21}+1) \cdot \left[1 - \frac{\frac{f_1 \cdot a_1}{f_4 \cdot a_4} \cdot k_{21}}{(2+f_1)\sqrt{1+\frac{(1+f_1)}{(2+f_1)}k_{21}}} \right]^{-(2+f_4)} \tag{C.6}$$

$$p_6(p_1) = p_4(p_1) \cdot \left[2\left(\frac{p_2(p_1)}{p_4(p_1)} \right)^{\frac{1}{2+f_4}} - 1 \right]^{2+f_4} \tag{C.7}$$

Appendix D. The relation $t_{FREC} = 2t_{FRE}$

In Fig. 3-6 maximum $\Delta_2 t$ is pictured at the point $x = x_{FREC} = x_{SR}$ at time $t_{FREC} = t_{SRC} = 2t_{FRE}$. It can be shown that $t_{FREC} = 2t_{FRE}$ and Fig. D-1 below shows the starting point.

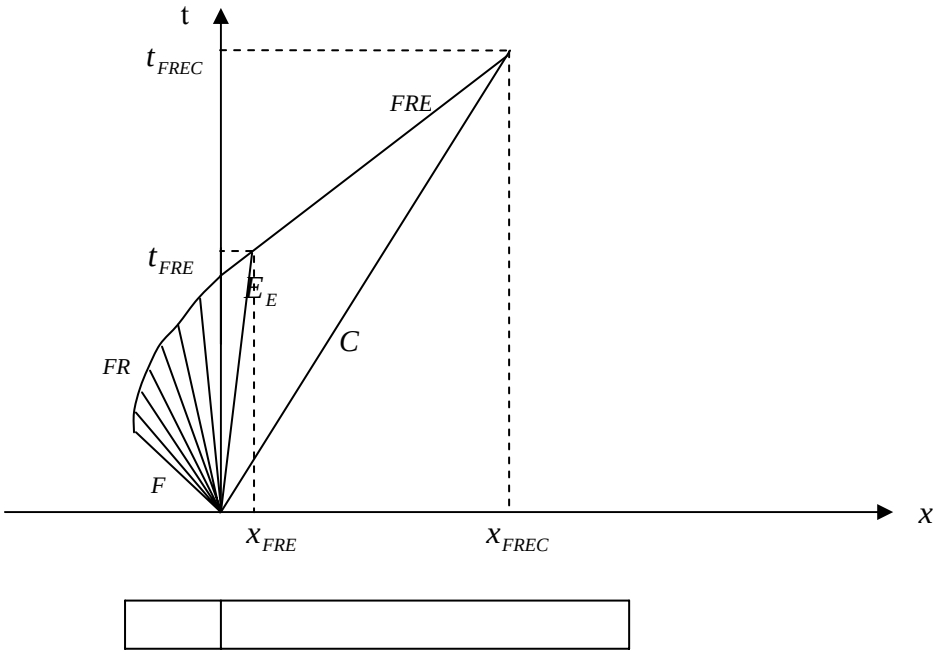

Figure D-1 Path (x) –Time (t) –diagram in purpose to determine the relationship between t_{FRE} and t_{FREC}.

The elapsed time t_{FRE} as the tale of the expansion wave E_E moving with the velocity u_{EE}, starting at origin and end up at the point x_{FRE} gives the distance

$$x_{FRE} = u_{EE} t_{FRE} = (u_3 - a_3) t_{FRE} \tag{D.1}$$

The elapsed time $t_{FREC} - t_{FRE}$ as the wave front FRE moving with the velocity u_{FRE}, starting at the point x_{FRE} and end up at the point x_{FREC} gives the distance

$$x_{FREC} - x_{FRE} = u_{FRE}(t_{FREC} - t_{FRE}) = (u_3 + a_3)(t_{FREC} - t_{FRE}) \tag{D.2}$$

The elapsed time t_{FREC} as the contact surface C moving with the velocity $u_p = u_3$, starting at origin and end up at the point x_{FREC} gives the distance

$$x_{FREC} = u_3 t_{FREC} \tag{D.3}$$

Further, the distance $x_{FREC} = x_{FREC} - x_{FRE} + x_{FRE}$ and by substitution with Eq. D.1-2 and using Eq. D.3 yields

$$u_3 t_{FREC} = (u_3 + a_3)(t_{FREC} - t_{FRE}) + (u_3 - a_3) t_{FRE} \tag{D.4}$$

Simplifying and solving for t_{FREC} finally gives the relation

$$t_{FREC} = 2t_{FRE} \tag{D.5}$$

which was to be shown.

Appendix E. Graphs

Graphs obtained for different combinations of gases by using the equations given in Appendix C and Eqs. 13 and 14, $T = 288.15K$ and $p_{5\max} = 40Mpa$. The restriction of $p_{4\max} = 40Mpa$ has been dropped since a comparison between different graphs would not be possible in some cases due to the fact that the ratio $p_{5\max} / p_{4\max} < 1$.

Graphs E1-E10 show maximum pressure steps and maximum pressures for different combinations of gases with respect to k_{21}. Values of k_{21} ensure a theoretical steady state in section (6).

Graphs E11-E30 show the coefficient of pressure step efficiency $c_{e,5}$ and $c_{e,2}$ compared with the ratio $p_{5\max} / p_{4\max}$ for different combinations of gases with respect to k_{51} and k_{21}, respectively.

The ranges of k_{21} and k_{51} within $p_{5\max} / p_{4\max} \geq 1$ are of particular interest.

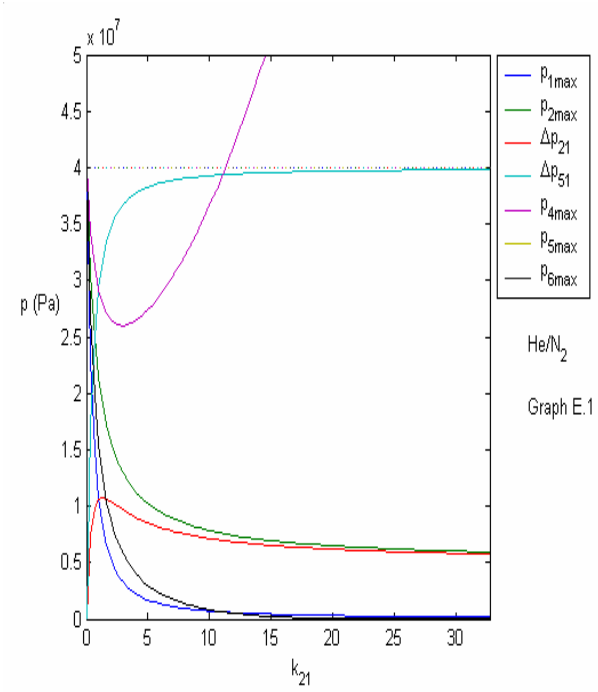

He/N_2

Graph E.1

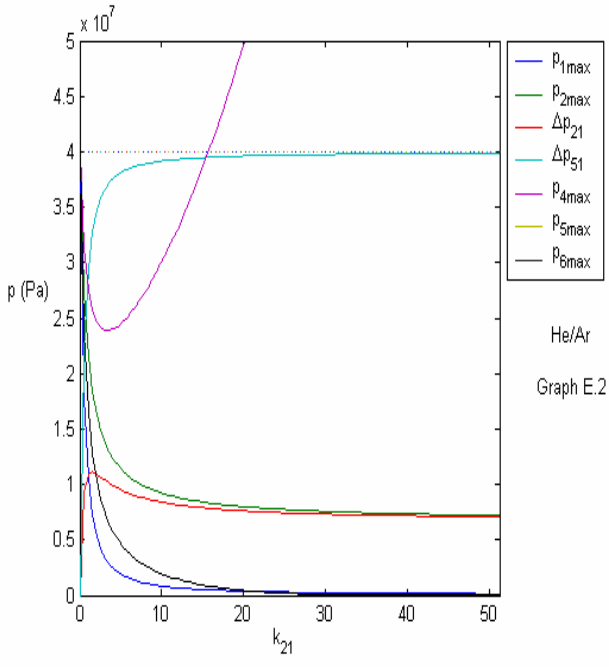

He/Ar

Graph E.2

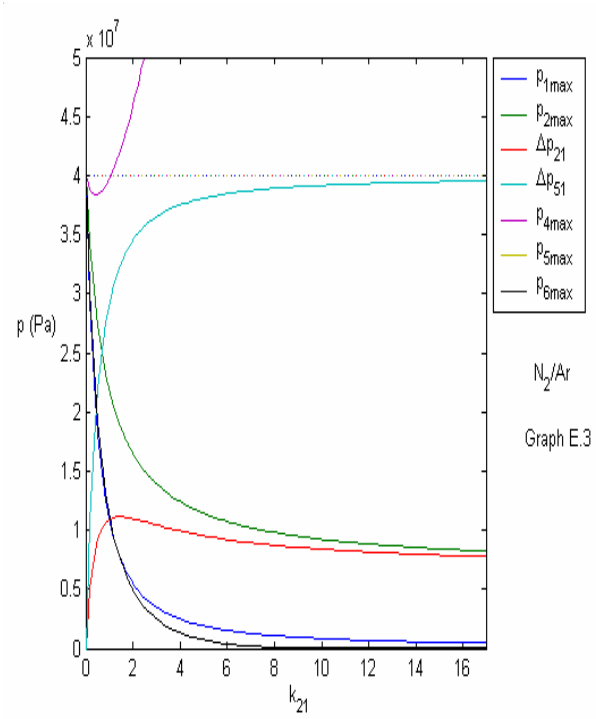

N_2/Ar

Graph E.3

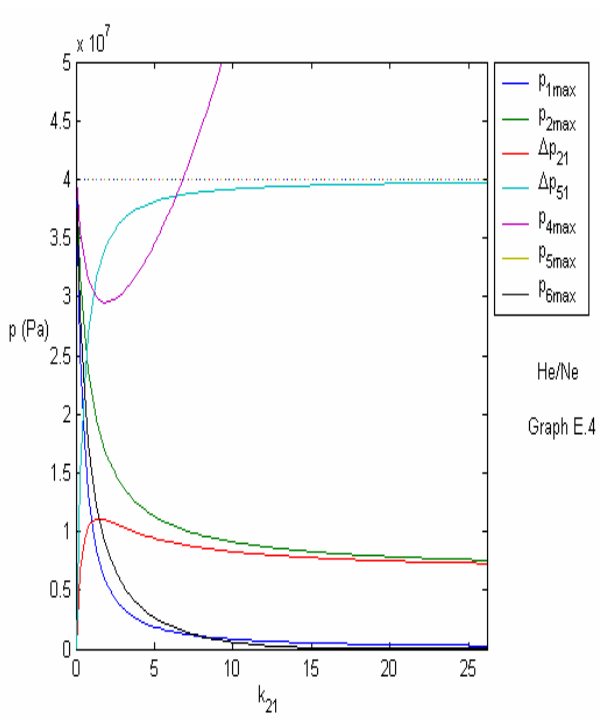

He/Ne

Graph E.4

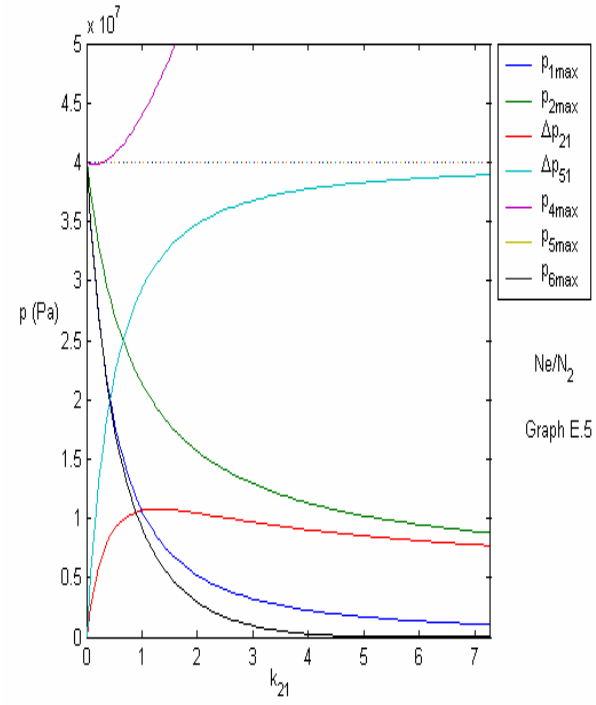

Ne/N_2

Graph E.5

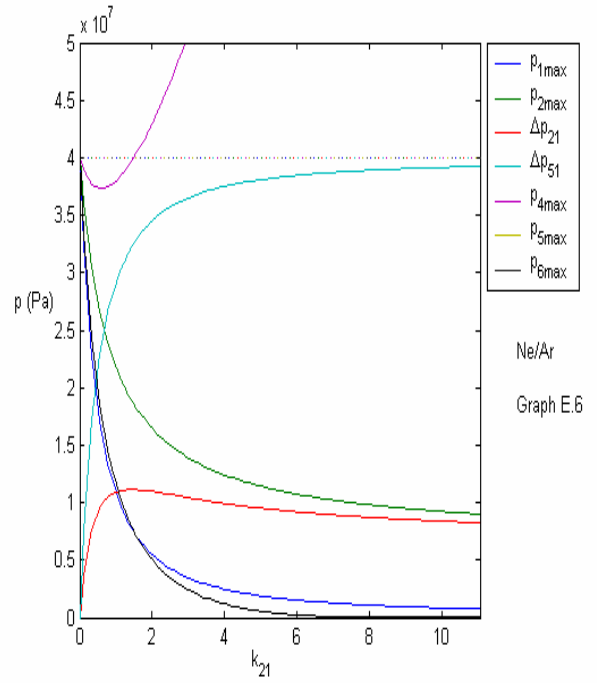

Ne/Ar

Graph E.6

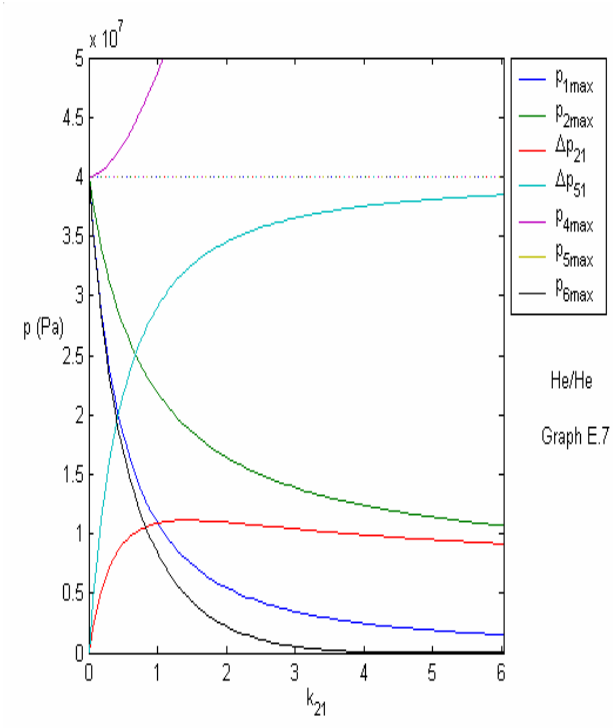

He/He

Graph E.7

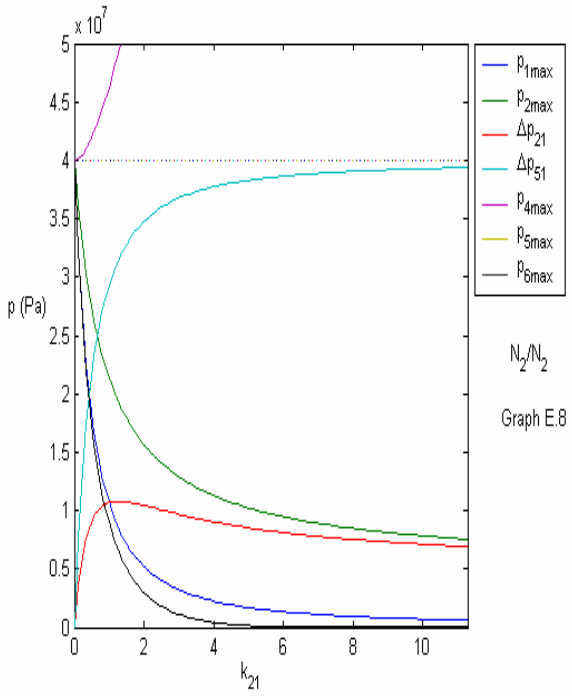

N_2/N_2

Graph E.8

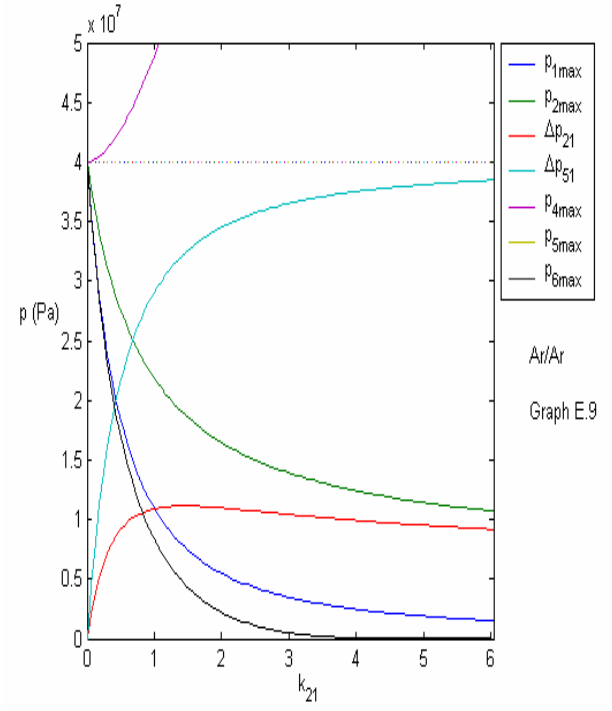

Ar/Ar

Graph E.9

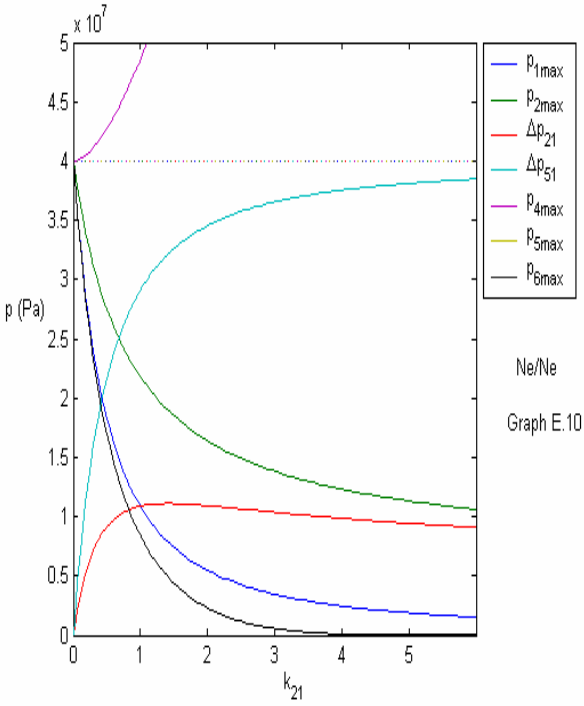

Ne/Ne

Graph E.10

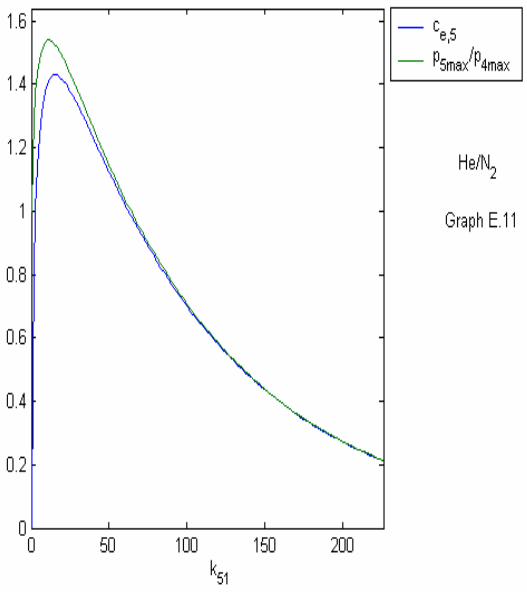

He/N_2

Graph E.11

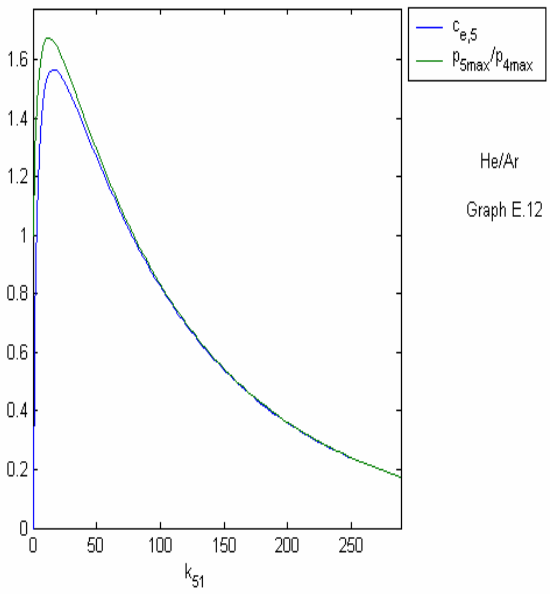

He/Ar

Graph E.12

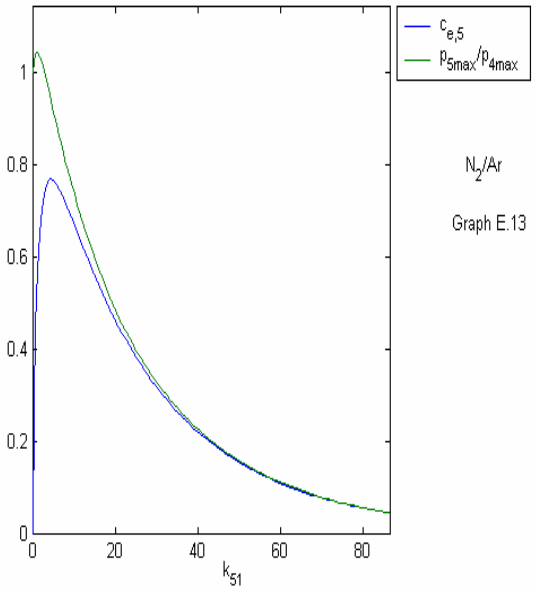

N_2/Ar

Graph E.13

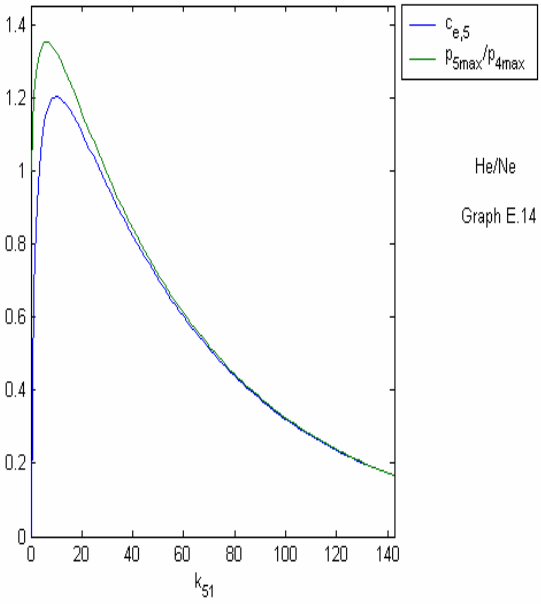

He/Ne

Graph E.14

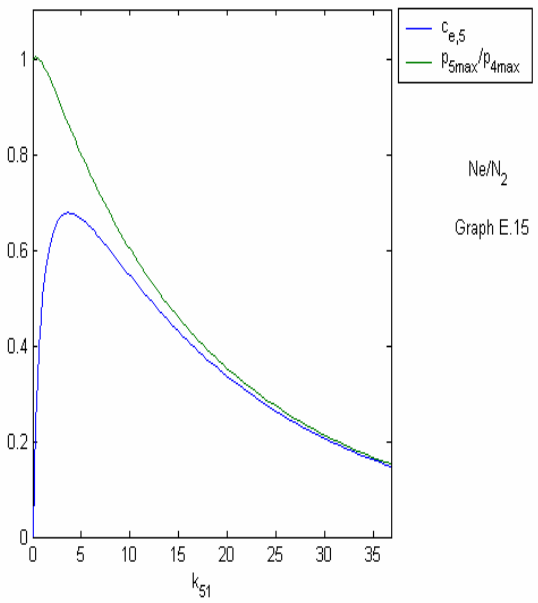

Ne/N_2

Graph E.15

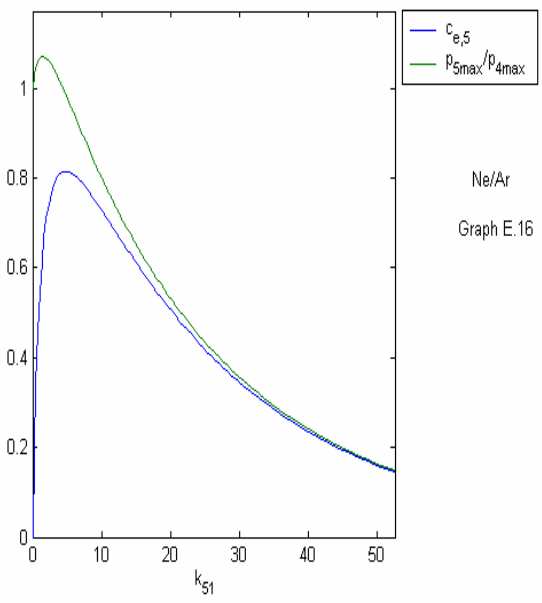

Ne/Ar

Graph E.16

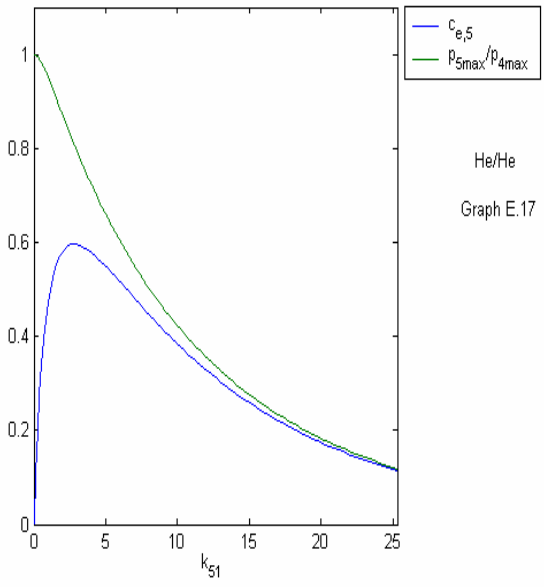

He/He

Graph E.17

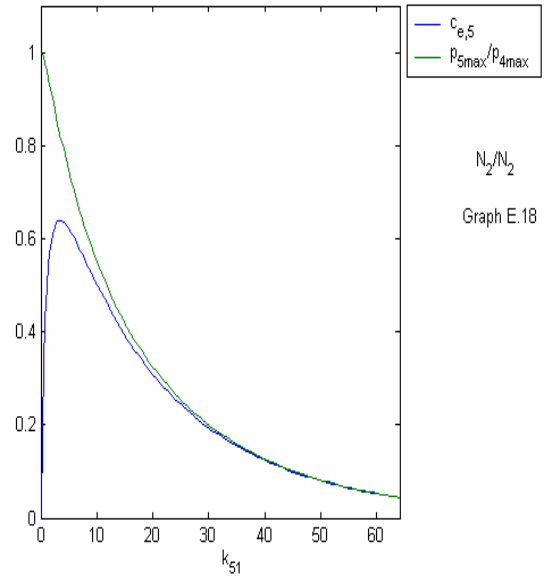

N_2/N_2

Graph E.18

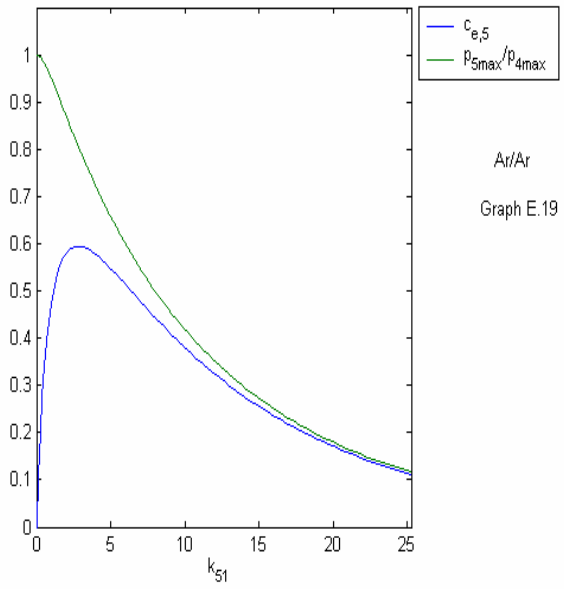

Ar/Ar

Graph E.19

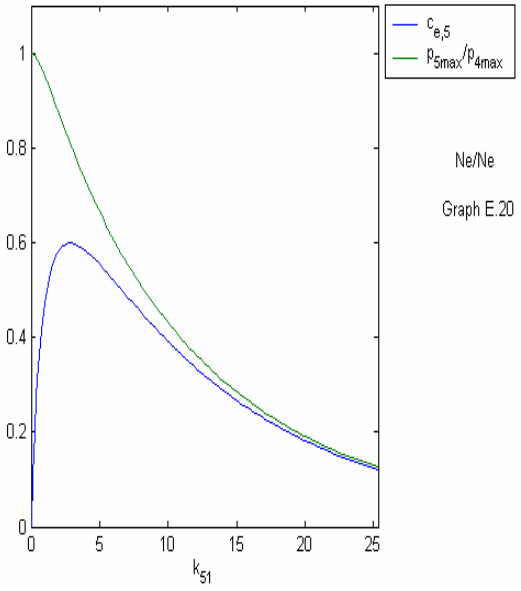

Ne/Ne

Graph E.20

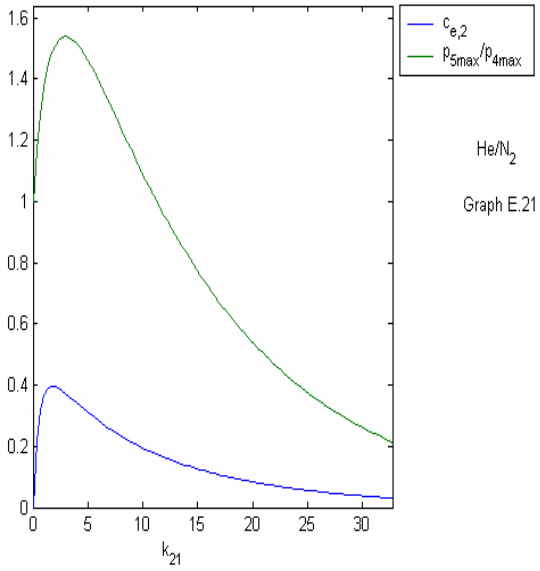

He/N_2

Graph E.21

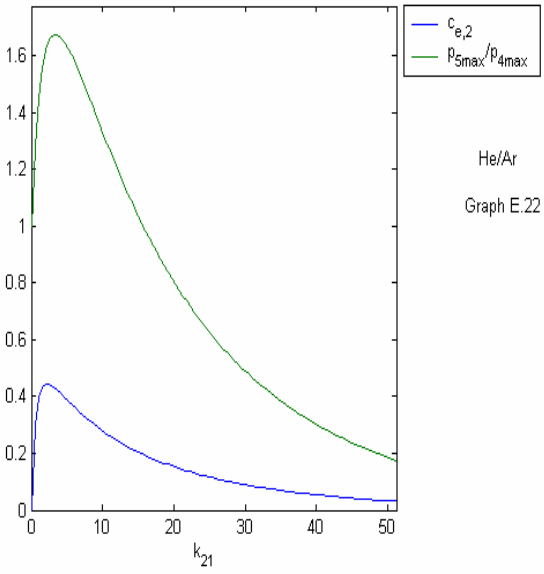

He/Ar

Graph E.22

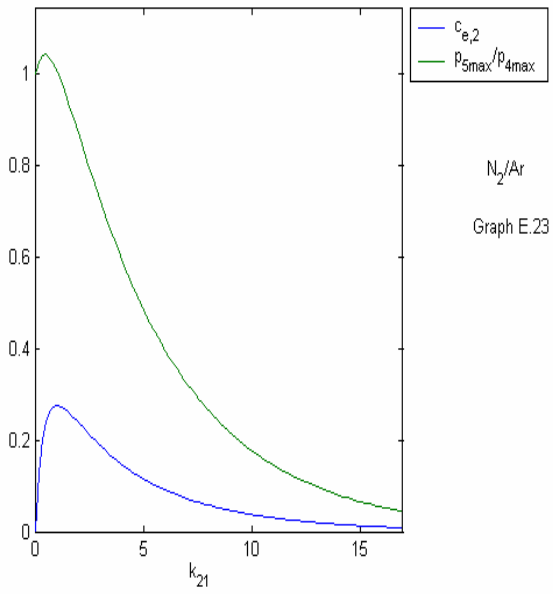

N_2/Ar

Graph E.23

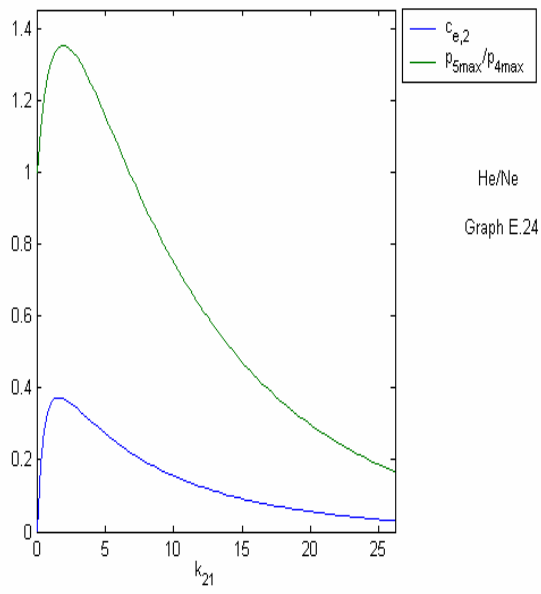

He/Ne

Graph E.24

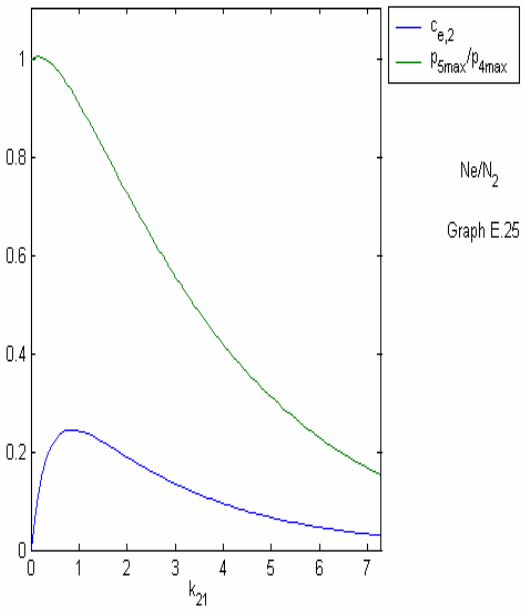

Ne/N_2

Graph E.25

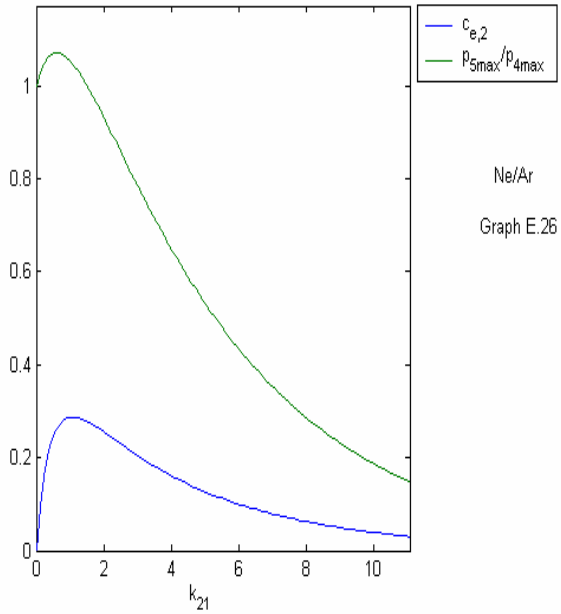

Ne/Ar

Graph E.26

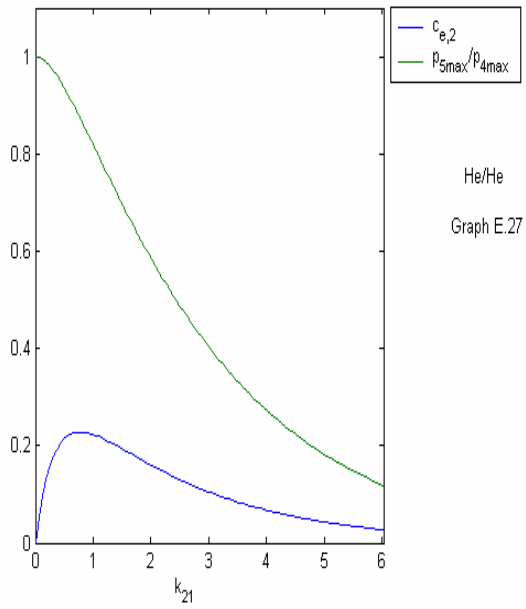

He/He

Graph E.27

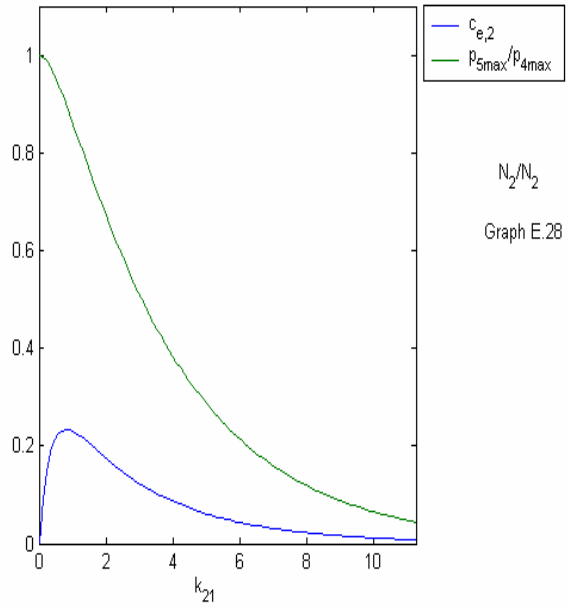

N_2/N_2

Graph E.28

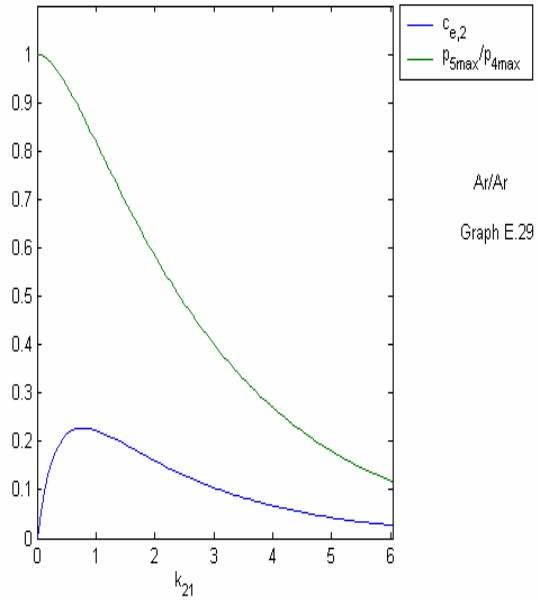

Ar/Ar

Graph E.29

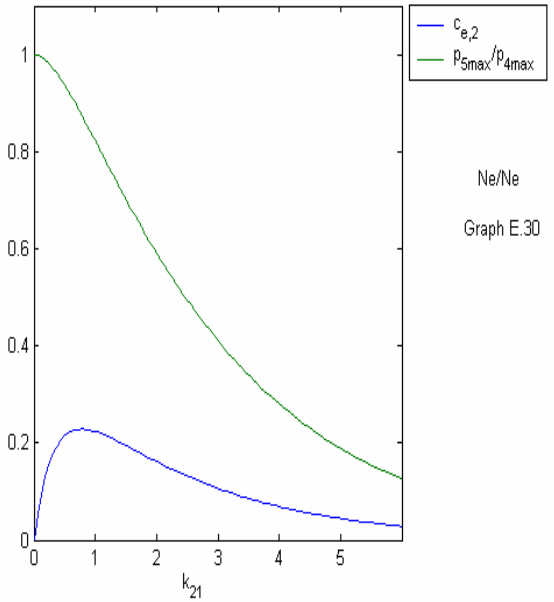

Ne/Ne

Graph E.30

Appendix F. Reynolds number as a transition number

A summary of the works of Mirels, [7] and [9] is given herein.

In sections (2) and (3) let the free stream Reynolds number be a transition number and thereby estimate where transition into turbulence occurs in the boundary layer at respective sections. The transition Reynolds number for incompressible flow over a semi-infinite flat plate $\mathrm{Re}_T = 0.5 \cdot 10^6$ will be used to estimate the transition point behind a shock wave. The characteristic-line geometry corresponding to ideal flow is shown in Fig. F-1.

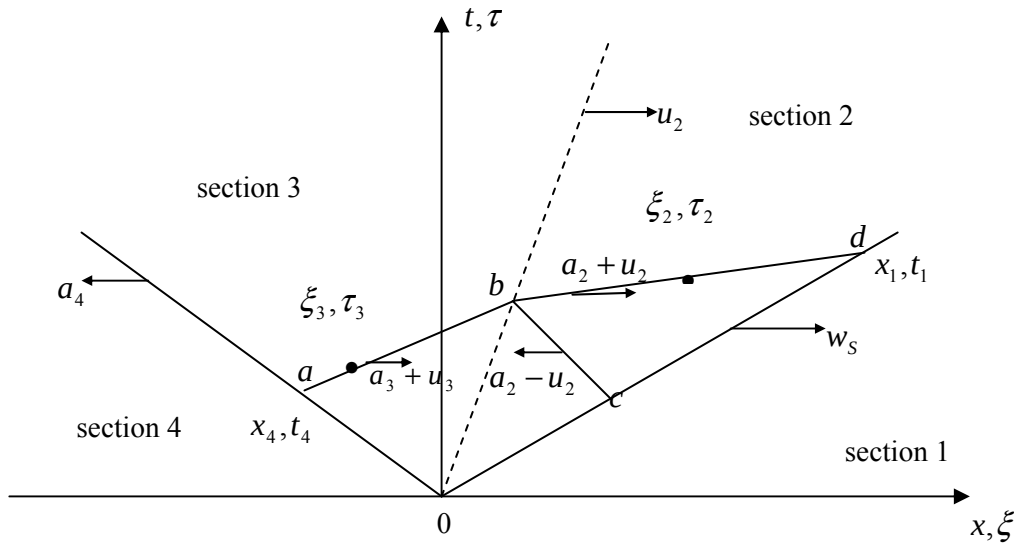

Figure F-1 Characteristic-line geometry.

The expansion wave is assumed to be of zero-thickness, i.e. an expansion shock wave. The point d with coordinates x_1, t_1 is assumed to be on the shock-wave characteristic and the point a with coordinates x_4, t_4 is assumed to be on the expansion-wave characteristic. The point b with coordinates x_b, t_b is assumed to be at the contact surface characteristic. ξ_2, τ_2 are coordinates of a point in section (2) and ξ_3, τ_3 are coordinates of a point in section (3).

$$\text{Section 2} \left(\frac{u_2}{w_S} \le \frac{\xi_2}{w_S \tau_2} \le 1 \right)$$

The Reynolds number characterizing the boundary-layer development in section (2) may be written as

$$\mathrm{Re}_2 = \frac{u_2 (w_S \tau_2 - \xi_2)}{\upsilon_2} \cdot \frac{\frac{u_2}{w_S}}{(1 - \frac{u_2}{w_S})} \tag{F.1}$$

for an arbitrarily basing υ_2 on free stream conditions. Let ξ_2, τ_2 be a point on the characteristic line through x_1, t_1. By using Eq. F.2 of the characteristic line bd into Eq. F.1

$$w_S\tau_2 - \xi_2 = \left[\frac{1+M_2-\left(\frac{w_S}{a_2}\right)}{1+M_2}\right](x_1-\xi_2) \tag{F.2}$$

The Reynolds number for points along line bd may be expressed as

$$\mathrm{Re}_2 = \frac{u_2(x_1-\xi_2)}{\upsilon_2}\cdot\left(\frac{\frac{u_2}{w_S}}{1-\frac{u_2}{w_S}}\right)\cdot\left(\frac{1+M_2-\frac{w_S}{a_2}}{1+M_2}\right) \tag{F.3}$$

From Eq. F.3 it is possible to determine the values of ξ_2 at which transition occurs, if a transition Reynolds number is known. In order to establish whether the boundary layer along the line bd is primarily laminar or turbulent let $\xi_2 = \xi_b$ and Eq. F.3 becomes

$$\mathrm{Re}_{2,b} = \frac{a_1 x_1}{\upsilon_1}\left[\upsilon_{12}\left(\frac{u_2}{w_S}\right)^2\left(1+M_2-\frac{w_S}{a_2}\right)M_S\right] \tag{F.4}$$

The maximum Reynold's number in section (2) occurs at the contact surface and in this case $\xi_2 = \xi_b$. The expression $\upsilon_{12} = \dfrac{\upsilon_1}{\upsilon_2}$.

$$\text{Section 3}\left(-1 \le \frac{\xi_3}{a_4\tau_3} \le \frac{u_3}{a_4}\right)$$

In the same manner as in section (2), the Reynolds number characterizing the boundary-layer development in section (3) may be written as

$$\mathrm{Re}_3 = \frac{u_3(a_4\tau_3+\xi_3)}{\upsilon_3}\cdot\frac{\frac{u_3}{a_4}}{1+\frac{u_3}{a_4}} \tag{F.5}$$

for an arbitrarily basing υ_3 on free stream conditions. Let ξ_3, τ_3 be a point on the characteristic line ab through x_4, t_4. By using the Eq. F.6 of the characteristic line ab and Eq. F.7 at point a into Eq. F.5

$$a_4\tau_3 + \xi_3 = \left(\frac{1+M_3+\frac{a_4}{a_3}}{1+M_3}\right)(\xi_3-\xi_a) \tag{F.6}$$

$$\xi_a = -x_1 \left[\frac{1 + M_2 - \frac{w_S}{a_2}}{1 + M_3 + \frac{a_4}{a_3}} \right] \frac{a_4}{w_S} \tag{F.7}$$

The Reynolds number for a point along the line ab influencing point x_1, t_1 may be expressed as

$$\mathrm{Re}_3 = \frac{u_3 x_1}{\upsilon_3} \frac{\frac{u_3}{a_4}}{1 + \frac{u_3}{a_4}} \frac{1 + M_3 + \frac{a_4}{a_3}}{1 + M_3} \left[\frac{\xi_3}{x_1} + \left(\frac{1 + M_2 - \frac{w_S}{a_2}}{1 + M_3 + \frac{a_4}{a_3}} \right) \frac{a_4}{w_S} \right] \tag{F.8}$$

In order to establish whether the boundary layer along ab is primarily laminar or turbulent let $\xi_3 = \xi_b$ and Eq. F.8 becomes

$$\mathrm{Re}_{3,b} = \frac{a_1 x_1}{\upsilon_1} \left[\upsilon_{13} \left(\frac{u_2}{w_S} \right)^2 \left(1 + M_2 - \frac{w_S}{a_2} \right) M_S \right] \tag{F.9}$$

The maximum Reynold's number in section (3) occurs at the contact surface and in this case $\xi_3 = \xi_b$. The expression $\upsilon_{13} = \frac{\upsilon_1}{\upsilon_3}$.

The relation between points along the line $0b$ and points along the line $0d$ is obtained by

$$\begin{aligned} t_b &= \frac{x_b}{u_2} \\ x_1 = t_b \cdot w_S \quad &\Rightarrow \quad x_1 = \frac{w_S}{u_2} x_b \end{aligned} \tag{F.10}$$

The relation between points along the line $0a$ and points along the line $0b$ is obtained by

$$\begin{aligned} t_b &= \frac{x_b}{u_2} \\ x_4 = t_b \cdot a_4 \quad &\Rightarrow \quad x_4 = \frac{a_4}{u_2} x_b \end{aligned} \tag{F.11}$$

The relation between points along the line $0a$ and points along the line $0d$ is obtained by

$$\begin{aligned} t_4 &= \frac{x_4}{a_4} \\ x_1 = t_4 \cdot w_S \quad &\Rightarrow \quad x_1 = \frac{w_S}{a_4} x_4 \end{aligned} \tag{F.12}$$

Appendix G. Thin turbulent boundary layer behind wave

A summary of the works of Mirels, [7] and [9] is given herein.
The theory of thin boundary layer behind a wave advancing into a stationary fluid is presented in [9]. The relevant coordinate system is fixed with respect to the wave and later transformed according to [7] with respect to the wall.
The expansion wave is assumed to be of zero-thickness i.e. an expansion shock, valid for weak expansion waves. The shock and expansion wave move with constant velocity, parallel to the wall, Fig. G-1.

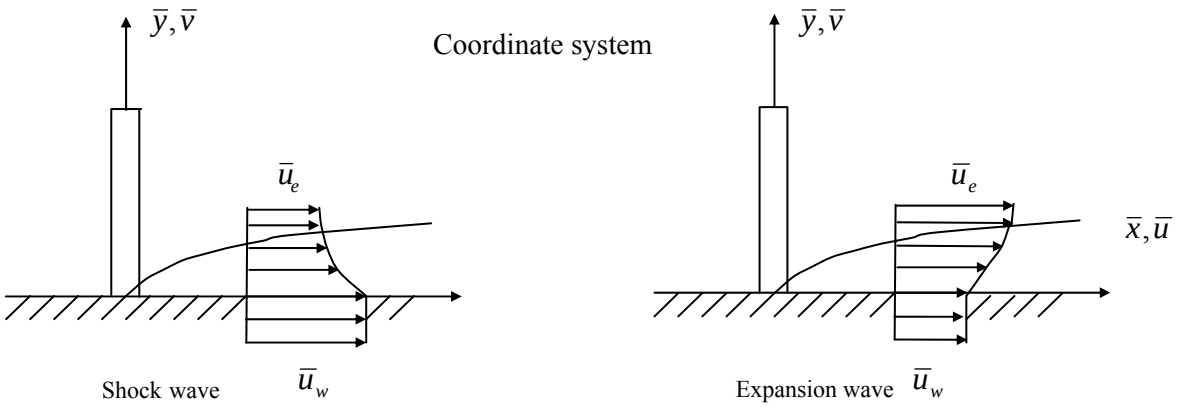

(a) with respect to wave

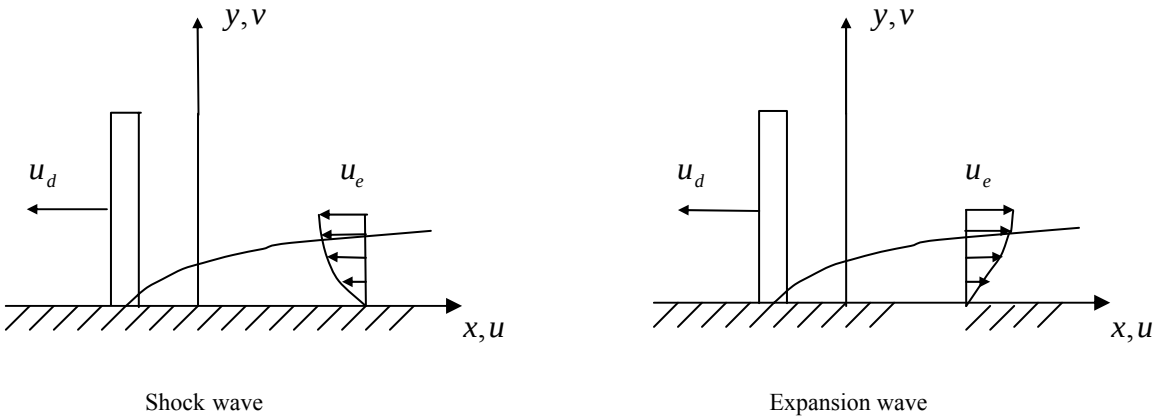

(b) With respect to wall

Figure G-1 Boundary layer behind a wave advancing into a stationary fluid.

The theory uses steady flow in its application where $\bar{x}, \bar{y}$ represents a coordinate system moving with the wave Fig.F1(a). The velocities $\bar{u}$ and $\bar{v}$ are parallel to the $\bar{x}$ - and $\bar{y}$ - coordinates. Fig.G-1 (b) represents a coordinate system fixed with respect to the wall and the velocities u and v are parallel to the coordinates x and y respective. Index e represents the free stream property and u_d is the velocity of the wave.

Assume that at time $t = 0$ the two coordinate systems coincide, the transformation relating the two systems can be expressed as

$$\begin{aligned} x &= \bar{x} - \bar{u}_w t \\ u &= \bar{u} - \bar{u}_w \\ y &= \bar{y} \\ v &= \bar{v} \end{aligned} \tag{G.1}$$

G.1 Thickness of turbulent boundary layer

The thickness of the boundary layer has its maximum at the contact surface. Section (2) i.e. with respect to the shock wave will be treated. The wall surface temperature is assumed to be constant.

By using the method employed for the solution of turbulent compressible flow over a semi-infinite flat plate and apply the method for the case of a moving wall, it is possible to obtain the thickness of a turbulent boundary layer. The equations of motion may be integrated over the $\bar{y}$-coordinate giving the relations between certain mean values of the boundary-layer properties.[28] The momentum and continuity equations will be treated in order to obtain a turbulent boundary-layer solution.

G.1.1 Equations of motion

In case of stationary flow of the free stream velocity $\bar{u}_e$, the velocity of the potential flow is constant and the pressure gradient $\frac{\partial p}{\partial \bar{x}}$ is taken as zero[29]. Using the Prandtl boundary-layer equations[30] for the flow in the vicinity of the wall, except at the base of the wave, the boundary layer equations of motion are, $(\bar{x} > 0)$

$$\begin{aligned} \frac{\partial \rho \bar{u}}{\partial \bar{x}} + \frac{\partial \rho \bar{v}}{d\bar{y}} &= 0 && \text{(continuity)} \\ \bar{u}\frac{\partial \bar{u}}{\partial \bar{x}} + \bar{v}\frac{\partial \bar{u}}{\partial \bar{y}} &= \frac{1}{\rho}\frac{\partial}{\partial \bar{y}}\left(\mu \frac{\partial \bar{u}}{\partial \bar{y}}\right) && \text{(momentum)} \\ \rho c_P \left(\bar{u}\frac{\partial T}{\partial \bar{x}} + \bar{v}\frac{\partial T}{\partial \bar{y}}\right) &= \frac{\partial}{\partial \bar{y}}\left(k\frac{\partial T}{\partial \bar{y}}\right) + \mu\left(\frac{\partial \bar{u}}{\partial \bar{y}}\right)^2 && \text{(energy)} \\ p &= \rho R T && \text{(state)} \end{aligned} \tag{G.2a-d}$$

With the boundary conditions for $\bar{x} > 0$

---

[28] [2], Ch. 13.9
[29] [11] Ch. IX.
[30] [9], [11] Ch. IX and Ch. VIII.

$$\bar{u}(\bar{x},0)=\bar{u}_w=-u_d=-w_S \qquad \bar{u}(\bar{x},\infty)=\bar{u}_e$$
$$\bar{v}(\bar{x},0)=0 \tag{G.3}$$
$$T(\bar{x},0)=T_w \qquad T(\bar{x},\infty)=T_e$$

The coefficient of viscosity μ is referred to a mean temperature, Eq. G.13.

G.1.2 Displacement thickness δ^* of the boundary layer[28]

The integral form of Eq. G.2a is

$$\int_0^{\bar{\delta}} \frac{\partial \rho\bar{v}}{\partial \bar{y}}\, d\bar{y} = (\rho\bar{v})_\delta = -\int_0^{\bar{\delta}} \frac{\partial \rho\bar{u}}{\partial \bar{x}}\, d\bar{y} \tag{G.4}$$

where $\bar{\delta}$ is the distance from the wall and beyond $\bar{u}=\bar{u}_e$ and $T=T_e$.

Let $\bar{u}$ and $\bar{u}_e$ represent the average velocity and $\rho_e\bar{u}_e$ is constant with respect to $\bar{x}$. Thus,

$$\int_0^{\bar{\delta}} \frac{\partial}{\partial \bar{x}}(\rho_e\bar{u}_e)d\bar{y}=0 \tag{G.5}$$

It is possible to extend the integration up to ∞ because of the properties for $\bar{y}>\bar{\delta}$: $\bar{u}=\bar{u}_e$ and $\rho=\rho_e$. Adding Eqs. G.4 and G.5 and simplify give

$$\frac{\bar{v}_e}{\bar{u}_e}=\frac{d}{d\bar{x}}\int_0^{\infty}\left(1-\frac{\rho\bar{u}}{\rho_e\bar{u}_e}\right)d\bar{y} \tag{G.6}$$

and δ^* is the integral expression with the dimension length. The boundary layer "displaces" the external flow and gives the flat plate an apparent thickness.

G.1.3 Momentum thickness θ of the boundary layer[28]

Eq. G2b may be written as

$$\frac{\partial \rho\bar{u}^2}{\partial \bar{x}}+\frac{\partial \rho\bar{v}\bar{u}}{\partial \bar{y}}=\frac{\partial \tilde{\tau}}{\partial \bar{y}} \tag{G.7}$$

where $\tilde{\tau}$ is the shearing stress.

The integral form of Eq. G.7 is

$$\int_0^{\bar{\delta}} \frac{\partial \rho\bar{u}^2}{\partial \bar{x}}\, d\bar{y}+\rho\bar{u}\bar{v}\Big|_0^{\bar{\delta}}=\tilde{\tau}\Big|_0^{\bar{\delta}} \tag{G.8}$$

and $\tilde{\tau}_{\bar{\delta}}=0$.

Using Eqs. G.8 and G.4, extend the limit of the integration and simplify give

$$\frac{\tilde{\tau}_w}{\rho_e\bar{u}_e^2}=\frac{d}{d\bar{x}}\int_0^{\infty}\frac{\rho\bar{u}}{\rho_e\bar{u}_e}\left(1-\frac{\bar{u}}{\bar{u}_e}\right)d\bar{y}=\frac{d\theta}{d\bar{x}} \tag{G.9}$$

This is the Kármán's momentum integral for compressible fluid flow past a flat plate and θ is the integral expression with the dimension length. Eq. G.9 expresses the skin friction (shearing

stress) at the wall as a "momentum defect". $\bar{u}/\bar{u}_e$ represents the average velocity and $\tilde{\tau}_w$ denotes the local shear stress exerted by fluid on wall.

G.1.4 Turbulent boundary layer solution

Define a similarity parameter $\zeta_T \equiv \frac{\bar{y}}{\tilde{\delta}}$ and $\tilde{\delta}$ is the boundary-layer thickness. It is assumed that $u/u_e = \zeta_T^{\frac{1}{7}}$ for $0 \le \zeta_T \le 1$. In case of a moving wall, assume that the velocity profiles have a seventh-power profile[31], which gives

$$0 \le \zeta_T \le 1, \qquad \left|\frac{\bar{u}-\bar{u}_w}{\bar{u}_e-\bar{u}_w}\right| = \zeta_T^{\frac{1}{7}}$$

$$1 \le \zeta_T, \qquad \left|\frac{\bar{u}-\bar{u}_w}{\bar{u}_e-\bar{u}_w}\right| = 1 \tag{G.10}$$

The ratio $\frac{T}{T_e}$ as a function of ζ_T may be expressed as

$$0 \le \zeta_T \le 1, \qquad \frac{\rho}{\rho_e} = \frac{T}{T_e} = \frac{T_w}{T_e}(1 + b\zeta_T^{\frac{1}{7}} - c\zeta_T^{\frac{2}{7}})$$

$$1 \le \zeta_T, \qquad \frac{\rho}{\rho_e} = \frac{T}{T_e} = 1 \tag{G.11}$$

where

$$b = \frac{T_r}{T_w} - 1 \qquad c = \left(\frac{T_r}{T_e} - 1\right)\frac{T_e}{T_w}$$

The recovery temperature T_r may be estimated as

$$\frac{T_r}{T_e} = 1 + \left(\frac{u_w}{u_e} - 1\right)^2 \frac{u_e^2 \sqrt[3]{\sigma_m}}{2T_e c_{p,m}} \tag{G.12}$$

Index m refers to a mean temperature T_m[32] and

$$T_m = 0.5(T_w + T_e) + 0.22(T_r - T_e) \tag{G.13}$$

The ratio $\frac{\theta}{\tilde{\delta}}$ is obtained by using Eqs. G.10 and G.11. Further, the ratio $\frac{\theta}{\tilde{\delta}}$ is independent of $\bar{x}$ which means that Eq. G.9 may be expressed as

---

[31] [14], Ch. XVI.
[32] [9], reference 13.

$$\frac{\tau_w}{\rho_e u_e^2} = \frac{\theta}{\tilde{\delta}} \frac{d\tilde{\delta}}{dx} \tag{G.14}$$

The relation between $\tilde{\tau}_w$ and $\tilde{\delta}$ is obtained according to the Blasius relation[33] and may be extended as an approximation into the case of compressible flow by the use of a suitable mean temperature T_m. For the case of a moving wall and using the velocities relative to the wall, Eq. G.14 can be written as

$$\frac{\tilde{\tau}_w}{\rho_e \bar{u}_e^2} = 0.0225\varphi\left(1-\frac{\bar{u}_w}{\bar{u}_e}\right)\left|1-\frac{\bar{u}_w}{\bar{u}_e}\right|^{\frac{3}{4}}\left(\frac{\upsilon_e}{\bar{u}_e\tilde{\delta}}\right)^{\frac{1}{4}} \tag{G.15}$$

where

$$\varphi = \left(\frac{\mu_m}{\mu_e}\right)^{\frac{1}{4}}\left(\frac{T_e}{T_m}\right)^{\frac{3}{4}}$$

and υ_e is the kinematic coefficient of viscosity.

Eq. G.15 into Eq. G.14, for T_w constant with respect to $\bar{x}$ and integration gives

$$\tilde{\delta} = 0.0574\left(\varphi\frac{1-\frac{\bar{u}_w}{\bar{u}_e}}{\frac{\theta}{\tilde{\delta}}}\right)^{\frac{4}{5}}\left|1-\frac{\bar{u}_w}{\bar{u}_e}\right|^{\frac{3}{5}}\left(\frac{\upsilon_e}{\bar{u}_e\bar{x}}\right)^{\frac{1}{5}}\bar{x} \tag{G.16}$$

The validity of Eq. G.16 depends on the Reynolds number[34] and if account has to be taken to Reynolds numbers of arbitrary magnitude, another estimation has to be used as a relation between $\tilde{\tau}_w$ and $\tilde{\delta}$. This may be the case according to Fig. 3.11.
From reference [13] the drag coefficient can be written as

$$c_f = 0.072\left(\frac{\upsilon_e}{u_e x}\right)^{\frac{1}{5}} \qquad 0.5\cdot 10^6 < \frac{u_e x}{\upsilon_e} = \mathrm{Re}_x < 10^7 \tag{G.17}$$

Eq. G.17 is based on the Blasius relation and is valid for Reynolds number up till an order of magnitude of 10^7. The Reynolds number of section (2) has that order of magnitude when the pressure p_1 is about $100kPa$, Fig. 3-10. In case of pressure of higher magnitude the thickness of turbulent boundary layer will be thinner. The case where the thickness of turbulent boundary layer has its maximum is of interest, i.e. $p_1 = 100kPa$. It is assumed herein that the Blasius relation is sufficient and no investigation of Reynolds number of arbitrary magnitude will be made in this report.

Transformation of Eq. G.16 into coordinates with respect to wall[35] at point b result into

---

[33] [13], Ch. XVI and Ch. XVII.
[34] [13], Ch. XVII.
[35] Appendix I.

$$\widetilde{\delta}_{2,b} = 0.0574\left(\varphi_2 \left[\frac{u_2 / w_S}{\frac{\theta_2}{\widetilde{\delta}_2}\left(\frac{u_2}{w_S} - 1 \right)} \right] \right)^{\frac{4}{5}} \left(\frac{u_2}{w_S} \right)^{\frac{3}{5}} \left(\frac{\upsilon_2}{w_S} \right)^{\frac{1}{5}} \cdot G^{\frac{4}{5}} \cdot x_1^{\frac{4}{5}} \qquad \text{(G.18)}$$

where

$$G = \frac{1 + M_2 - \frac{w_S}{a_2}}{1 + M_2} \qquad \varphi_2 = \left(\frac{\mu_{2,m}}{\mu_2} \right)^{\frac{1}{4}} \left(\frac{T_2}{T_{2,m}} \right)^{\frac{3}{4}} \qquad \text{(G.18a)}$$

and

$$\frac{\theta_2}{\widetilde{\delta}_2} \frac{\frac{u_2}{w_S} - 1}{u_2 / w_S} = \frac{7 \frac{T_2}{T_1} \left[I_{2,6} - \left(1 + \frac{u_2}{w_S} \right) I_{2,7} + \frac{u_2}{w_S} I_{2,8} \right]}{1 - (u_2 / w_S)} \qquad \text{(G.18b)}$$

where $T_1 = T_{2,w}$ refers to the wall temperature[36], I_6, I_7 and I_8 are functions of b and c defined by the integral

$$\begin{aligned} I_{2,N} &= \int_0^1 \frac{z^N}{1 + b_2 z - c_2 z^2} dz \\ b_2 &= \frac{T_{2,r}}{T_1} - 1 \\ c_2 &= \left(\frac{T_{2,r}}{T_2} - 1 \right) \left(\frac{T_2}{T_1} \right) \\ \frac{T_{2,r}}{T_2} &= 1 + f_1^{-1} M_2^2 (\sigma_2)^{\frac{1}{3}} \\ \frac{T_{2,m}}{T_2} &= 0.5 \left(\frac{T_1}{T_2} + 1 \right) + 0.22 \left(\frac{T_{2,r}}{T_2} - 1 \right) \end{aligned} \qquad \text{(G.18c)}$$

$\widetilde{\delta}_{2,b}$ is the thickness of turbulent boundary layer at the contact surface with respect to section (2) and x_1 refers to the shock wave.

[36] [7], p.30

Appendix H. Approximation of $\sigma, \mu, c_p, \rho, \upsilon$ and k_h

All the data will be taken from [12] in the case of Helium in section (3) and Argon in section (2). Using Matlab(Math Works) 'polyfit-function', least square solutions are obtained fitted the data with respect to the pressure p_1. The solutions will be polynomials.

The pressure p_1 will act as a parameter indicating a variation of the Prandtl number σ, the coefficient of viscosity μ, specific heat of constant pressure c_p, the kinematic coefficient of viscosity υ and the coefficient of heat conductivity k_h. The Prandtl number and the kinematic coefficient of viscocity are defined as

$$\sigma = \frac{\mu}{k_h} c_p \qquad \upsilon = \frac{\mu}{\rho} \tag{H.1}$$

From Eq (H.1)

$$\frac{1}{\upsilon_1} \cdot \frac{\upsilon_1}{\upsilon_2} = \frac{\rho_2}{\rho_1} \cdot \frac{\rho_1}{\mu_2} \qquad \frac{1}{\upsilon_1} \cdot \frac{\upsilon_1}{\upsilon_3} = \frac{\rho_3}{\rho_1} \cdot \frac{\rho_1}{\mu_3} \tag{H.2}$$

The relations state with $i = 2$ and 3

$$\begin{aligned}
&\sigma_i = \sigma_i(\mu_i, k_{h,i}, c_{p,i}) && \upsilon_i = \upsilon_i(\mu_i, \rho_i) \\
&c_{p,i} = c_{p,i}(T_i, p_i) && \mu_i = \mu_i(T_i, p_i) \\
&p_i = p_i(p_1, k_{21}) && T_i = T_i(k_{21}, \gamma_{1,4}, T_{1,4}) \\
&\rho_i = \rho_i(\rho_{1,4}, k_{21}, \gamma_{1,4}) && \rho_{1,4} = \rho_{1,4}(p_1, T_{1,4}) \\
&k_{h,i} = k_{h,i}(T_i, p_i)
\end{aligned} \tag{H.3}$$

For $k_{21} = 2.18$ and with He/Ar as chosen gas combination, the temperatures T_i will be constant, $T_2 = 480K$ and $T_3 = 243K$ using equations in Table. A-1 and Table A-5.
$T_1 = T_4 = 288.15K$.
The mean temperature $T_{2,m}$ was evaluated using equations in App. G. It was found that $T_{2,m}$ was kept at ~ $395K$ over the interval $100kPa \le p_2 \le 20MPa$.
In order to find the free stream values of μ_2 and μ_3 at the temperatures T_2 and T_3 respective, several polynomials were fitted to the data presented in [12]. The procedure was done for different values of temperature with respect to values of μ_2 and μ_3 keeping each different pressure p_2 constant (at contact surface $p_2 = p_3$). Further, two polynomials were fitted to the values of μ_2 and μ_3 corresponding to T_2 and T_3 respective. These two polynomials were used to obtain values of μ_2 and μ_3 up till $p_2 = 20Mpa$.
Values of $k_{h,2}$ and $\mu_{2,m}$ were obtained in the same way.
Values of $c_{p,2}$, data was directly taken from [12] within temperature range of
$450K < T_2 < 500K$, then a polynomial was fitted with respect to the pressure range.
In the case of Argon, the interval of temperature used was $250K \le T_2 \le 600K$ and the interval of pressure used was $100kPa \le p_2 \le 20MPa$.

In the case of Helium the interval of temperature used was $100K \le T_3 \le 400K$ and the interval of pressure used was $100kPa \le p_2 \le 20MPa$.
To find the values of ρ_1 with respect to p_1, a polynomial was fitted to the data presented in [12] and the interval of pressure used was $50kPa \le p_1 \le 20MPa$ under the condition $T_1 = 288.15K$.

The resulting polynomials as a function of p_1, may then be expressed as

$$\begin{aligned}
&\rho_1(T_1 = 288.15K) = -4.46\cdot10^{-21}\cdot {p_1}^3 + 1.42\cdot10^{-13}\cdot {p_1}^2 + 1.66\cdot10^{-5}\cdot p_1 + 1.77\cdot10^{-2}\\
&\mu_2(T_2 = 480K) = 3.51\cdot10^{-21}((k_{21}+1)p_1)^2 + 5.33\cdot10^{-14}(k_{21}+1)p_1 + 3.20\cdot10^{-5}\\
&\mu_3(T_3 = 243K) = 6.72\cdot10^{-22}((k_{21}+1)p_1)^2 + 2.42\cdot10^{-14}(k_{21}+1)p_1 + 1.76\cdot10^{-5}\\
&k_{h,2}(T_2 = 480K) = 5.29\cdot10^{-19}((k_{21}+1)p_1)^2 + 2.56\cdot10^{-10}(k_{21}+1)p_1 + 2.50\cdot10^{-2}\\
&c_{p,2}(T_2 = 480K) = 1.42\cdot10^{-20}((k_{21}+1)p_1)^3 - 3.94\cdot10^{-13}((k_{21}+1)p_1)^2 +\\
&\qquad 5.84\cdot10^{-6}(k_{21}+1)p_1 + 5.17\cdot10^{2}\\
&\mu_{2,m}(T_{2,m} = 395K) = -2.30\cdot10^{-28}((k_{21}+1)p_1)^3 + 1.22\cdot10^{-20}((k_{21}+1)p_1)^2 +\\
&\qquad 2.98\cdot10^{-14}((k_{21}+1)p_1) + 2.79\cdot10^{-5}.
\end{aligned} \tag{H.4}$$

and $k_{21} = 2.18$.

Appendix I. Transformation equations

In Appendix G Eq. G.16 was transformed into Eq. G.18 and it is valid for coordinates with respect to wall. Transformation was made from coordinates with respect to wave into coordinates with respect to wall using equations below[37].

Region 2

$$\bar{u}_w = w_S \qquad \frac{\bar{u}_w}{\bar{u}_e} = \frac{1}{1-\frac{u_2}{w_S}}$$

$$\bar{u}_e = w_S - u_2 \qquad \frac{\bar{u}_w}{\bar{u}_e} - 1 = \frac{\frac{u_2}{w_S}}{1-\frac{u_2}{w_S}} \tag{I.1}$$

$$\bar{v}_e = v_2 \qquad \bar{x} = w_S \tau - \xi$$

$\tilde{\delta}_2$ at point b is found by the relation

$$\bar{x} = \frac{1+M_2-\frac{u_2}{w_S}}{1+M_2} \cdot \left(1-\frac{u_2}{w_S}\right) \cdot x_1 \tag{I.2}$$

[37] [7], App. D.

SP Swedish National Testing and Research Institute develops and transfers technology for improving competitiveness and quality in industry, and for safety, conservation of resources and good environment in society as a whole. With Swedens widest and most sophisticated range of equipment and expertise for technical investigation, measurement, testing and certfication, we perform research and development in close liaison with universities, institutes of technology and international partners.

SP is a EU-notified body and accredited test laboratory. Our headquarters are in Borås, in the west part of Sweden.

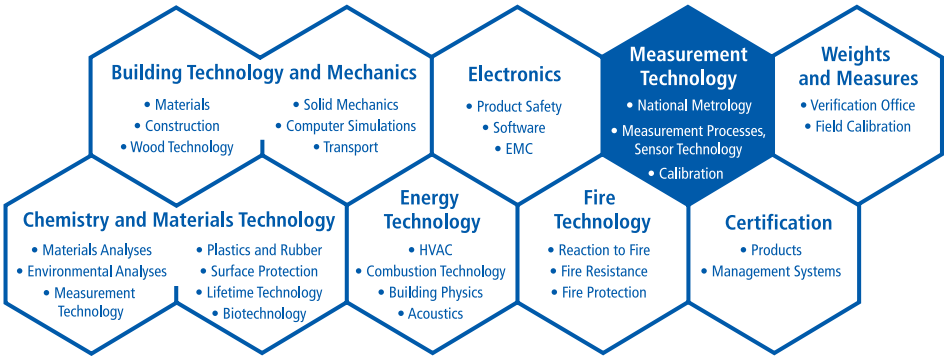

SP Measurement Technology
SP REPORT 2005:35
ISBN 91-85303-66-6
ISSN 0284-5172

SP Swedish National Testing and Research Institute
Box 857
SE-501 15 BORÅS, SWEDEN
Telephone: + 46 33 16 50 00, Telefax: +46 33 13 55 02
E-mail: info@sp.se, Internet: www.sp.se